Article

Current Biology

Light-sensitive short hypocotyl genes confer symbiotic nodule identity in the legume *Medicago truncatula*

Graphical abstract

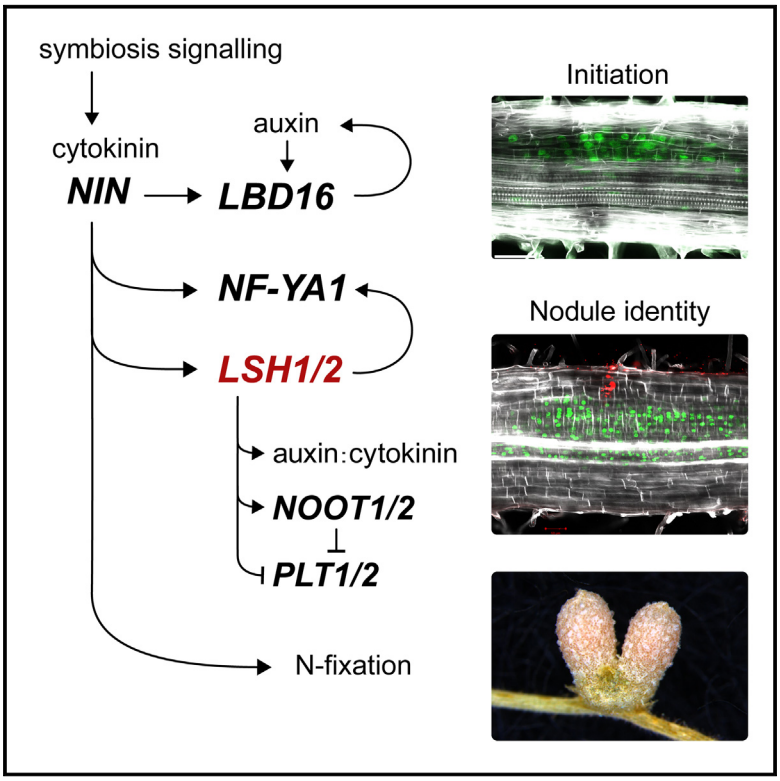

Highlights

- *LSHs* are key regulators of symbiotic root nodule differentiation downstream of *NIN*
- *LSHs* promote cell divisions in the root cortex that support bacterial colonization
- *LSHs* promote expression of the nodule organ identity genes *NOOT1/NOOT2* and *NF-YA1*
- *LSHs* repress *PLETHORA* root regulators and modulate auxin-cytokinin dynamics

Authors

Tak Lee, Martina Orvosova, Morgane Batzenschlager, ..., Thomas Ott, Giles E.D. Oldroyd, Katharina Schiessl

Correspondence

gedo2@cam.ac.uk (G.E.D.O.), katharina.schiessl@slcu.cam.ac.uk (K.S.)

In brief

To host N-fixing bacteria, legumes grow root nodules initiated via a lateral root program. Lee et al. show that two *LSH* transcription factors mediate the divergence between lateral roots and nodules by promoting the proliferation of colonizable cells. *LSH1/LSH2* regulate the nodule identity genes *NF-YA1* and *NOOT1/NOOT2* and auxin/cytokinin dynamics.

Lee et al., 2024, Current Biology *34*, 825–840
February 26, 2024
https://doi.org/10.1016/j.cub.2024.01.018

CellPress

Current Biology

CellPress
OPEN ACCESS

Article

Light-sensitive short hypocotyl genes confer symbiotic nodule identity in the legume *Medicago truncatula*

Tak Lee,[1,2,8,10] Martina Orvosova,[1,2,10] Morgane Batzenschlager,[3] Marcelo Bueno Batista,[4] Paul C. Bailey,[5] Nadia A. Mohd-Radzman,[1] Aram Gurzadyan,[1] Naomi Stuer,[1] Kirankumar S. Mysore,[6,9] Jiangqi Wen,[6,9] Thomas Ott,[3,7] Giles E.D. Oldroyd,[1,2,*] and Katharina Schiessl[1,11,12,*]

[1]Sainsbury Laboratory, University of Cambridge, 47 Bateman Street, Cambridge CB2 1LR, UK
[2]Crop Science Centre, Department of Plant Sciences, University of Cambridge, 93 Lawrence Weaver Road, Cambridge CB3 0LE, UK
[3]University of Freiburg, Faculty of Biology, Schänzlestrasse, 79104 Freiburg, Germany
[4]Department of Molecular Microbiology, John Innes Centre, Norwich Research Park, Norwich NR4 7UH, UK
[5]Jodrell Laboratory, Royal Botanic Gardens, Kew, Richmond TW9 3DS, UK
[6]Noble Research Institute, LLC, 2510 Sam Noble Parkway, Ardmore, OK 73401, USA
[7]CIBSS – Centre of Integrative Biological Signalling Studies, University of Freiburg, Schänzlestrasse, 79104 Freiburg, Germany
[8]Present address: Max Planck Institute for Plant Breeding Research, Carl-von-Linne-Weg, 1050829 Cologne, Germany
[9]Present address: Oklahoma State University, Stillwater, OK 74078, USA
[10]These authors contributed equally
[11]X (formerly Twitter): @kathschiessl
[12]Lead contact
*Correspondence: gedo2@cam.ac.uk (G.E.D.O.), katharina.schiessl@slcu.cam.ac.uk (K.S.)
https://doi.org/10.1016/j.cub.2024.01.018

SUMMARY

Legumes produce specialized root nodules that are distinct from lateral roots in morphology and function, with nodules intracellularly hosting nitrogen-fixing bacteria. We have previously shown that a lateral root program underpins nodule initiation, but there must be additional developmental regulators that confer nodule identity. Here, we show two members of the *LIGHT-SENSITIVE SHORT HYPOCOTYL* (*LSH*) transcription factor family, predominantly known to define shoot meristem complexity and organ boundaries, function as regulators of nodule organ identity. In parallel to the root initiation program, *LSH1/LSH2* recruit a program into the root cortex that mediates the divergence into nodules, in particular with cell divisions in the mid-cortex. This includes regulation of auxin and cytokinin, promotion of *NODULE ROOT1/2* and *Nuclear Factor YA1*, and suppression of the lateral root program. A principal outcome of *LSH1/LSH2* function is the production of cells able to accommodate nitrogen-fixing bacteria, a key feature unique to nodules.

INTRODUCTION

To overcome nitrogen (N) deficiencies in the soil, legumes have evolved the ability to enter symbioses with beneficial N-fixing rhizobial bacteria. Legumes accommodate rhizobia inside cells of specialized root organs called nodules, which provide a favorable environment for N fixation.

Initiation and progression of bacterial infection and nodule development are controlled by and dependent on the function of the nodulation-specific transcriptional regulator *NODULE INCEPTION* (*NIN*), which is activated downstream of the symbiosis signaling pathway.[1–3] Epidermal infection and nodule organogenesis are genetically separable processes as evidenced by studies of different *nin* loss-of-function alleles and studies of the *cis*-regulatory elements in the *NIN* promoter.[2–7] To initiate the development of symbiotic root nodules in the inner tissue layers, *NIN* expression is activated via *CYTOKININ RESPONSE 1* (*CRE1*)-mediated cytokinin signaling.[7,8] Our previous work showed that cytokinin-induced *NIN* recruits a conserved program associated with lateral root development, to initiate the formation of a symbiotic root nodule, through the transcriptional regulator *LATERAL ORGAN BOUNDARIES 16* (*LBD16*), which promotes cell proliferation in the inner tissue layers via the upregulation of *STYLISH-like* (*STY-l*) transcriptional regulators and *YUCCA* (*YUC*) auxin biosynthesis genes.[9,10] Consequently, nodules and lateral roots initiate from the same inner tissue layers of the primary root, including the pericycle, the endodermis, and the inner cortex, in response to the local accumulation of auxin.[9,11]

The commonalities between lateral root and nodule initiation imply that additional nodule-specific regulatory pathways must be recruited to confer nodule organ identity, in order to differentiate nodules from lateral roots in both morphology and function. While lateral root primordia predominantly develop from cells that are derived from the inner cell layers, the development of nodule primordia is in addition associated with the promotion of cell proliferation in the mid-cortex.[9–13] These cortical-derived primordial cells are key determinants in the establishment of nodule organ identity as they give rise to the cells that are intracellularly colonized by rhizobial bacteria, released from infection threads.[12]

Several regulators have been implicated in the promotion of cortical cell divisions downstream of cytokinin-induced *NIN* expression. These include the transcriptional regulator *NUCLEAR FACTOR YA1* (*NF-YA1*) and *NODULE ROOT1/2* (*NOOT1/NOOT2*), two broad-complex, tramtrack, and bric a brac (BTB)-ankyrin transcriptional co-activators orthologous to the *Arabidopsis* genes *BLADE-ON-PETIOLE 1/2* (*BOP1/2*).[12,14–17] *NF-YA1* functions in cortical infection thread progression, nodule initiation, and the subsequent establishment and maintenance of the nodule meristem, which provides cells for continued rhizobial infection in the indeterminate nodule of *Medicago truncatula* (*M. truncatula*).[10,12,17,18] *NF-YA1* acts in part through the upregulation of *STY* transcription factors and *YUC* auxin biosynthesis genes.[19,20] *NOOT1/NOOT2* appear to suppress the root-like initiation program induced by *NIN* via *LBD16* during nodule differentiation, with the *noot1/noot2* loss-of-function mutant developing root-like conversions from nodules.[9,14,15] While nodule development is compromised in *nf-ya1* and *noot1/noot2*, nodules still initiate in these mutants, which can at least in part support rhizobial colonization and N fixation, suggesting that additional regulators of nodule organ identity must act either upstream, redundantly, or in parallel with these known regulators. In this study, we demonstrate that two members of the *LIGHT-SENSITIVE SHORT HYPOCOTYL* (*LSH*) transcription factor family that previously have been shown to predominantly control shoot meristem function also control nodule organ identity downstream of *NIN*. These genes are required to provide the unique organ identity of nodules, allowing intracellular bacterial colonization and N fixation. Through the transcriptional control of and together with the known nodule organ identity regulators *NF-YA1* and *NOOT1/NOOT2*, *LSH1/LSH2* directly and indirectly recruit a growth-regulatory and differentiation program, highlighting the importance of the auxin-cytokinin crosstalk and the pleiotropic function of shoot- and nodule-expressed meristem and growth regulators in the specification of this symbiotically induced root organ.

RESULTS

LSH1 and *LSH2* are upregulated during early nodule organogenesis downstream of *NIN*

To define potential regulators of nodule organ identity, we screened a preexisting comparative RNA sequencing (RNA-seq) time course of nodule and lateral root development for transcription factors induced during the early stages of nodule development, with nodule-specific expression, in a manner dependent on *NIN*.[9,21] This selection criteria identified *NF-YA1*, its interacting subunit *NF-YB16* and *NOOT1/NOOT2*,[15,22,23] as well as two transcriptional regulators with yet uncharacterized functions in rhizobial symbiosis (Figure 1A). These novel regulators share an Arabidopsis LSH1 and oryza G1 (ALOG) domain of identical amino acid sequence, with high sequence similarity to *LSH* transcription factor 3 in *Arabidopsis* (*AtLSH3*) and with the recently characterized *SYMMETRIC PETALS 1* gene in *Pisum sativum* (*PsSYP1*) (Figure S1A).[24–26] We named these two genes *LSH1* and *LSH2*. *LSH1* and *LSH2* are upregulated in roots from 16 and 24 h post rhizobial spot inoculation (hpi), respectively. By contrast, neither *LSH1* nor *LSH2* was differentially expressed during the initiation and early development of lateral roots, suggesting that *LSH1* and *LSH2* may be part of a developmental program that distinguishes nodules from lateral roots (Figure 1A).[9] The expression of *LSH1* and *LSH2* during rhizobial infection was dependent on *CRE1* and *NIN*; ectopic expression of *NIN* was sufficient to upregulate both genes (Figure 1A),[9,21] and cytokinin treatment of *M. truncatula* roots induced *LSH1* in a *CRE1*- and *NIN*-dependent but *NF-YA1*-independent manner (Figure 1B). Furthermore, a high-confidence NIN DNA-binding site (found in three out of three biological replicates), 5,260 bp upstream of the transcription start site (TSS) of *LSH1*, was identified by chromatin immunoprecipitation (ChIP) in roots expressing *pLjUBI:GFP-NIN*, suggesting that *LSH1*, but not *LSH2*, is a direct target of NIN regulation (Figures S1B and S1C; Data S2A).

To investigate their spatial expression patterns, we performed mRNA *in situ* hybridization using antisense probes for *LSH1* and *LSH2* on wild-type (WT) root tissue 72 hpi, alongside *LSH* promoter-β-glucuronidase (GUS) analysis. Together, these approaches revealed that both genes are specifically expressed in dividing and newly divided cells of the nodule primordia, with no expression being observed in the overlaying outer cortical and epidermal cell layers that are traversed by infection threads (Figures 1C and 1D). In mature nodules, *LSH1* and *LSH2* are strongly expressed in the apical meristem region, in the infection and fixation zones, and in the peripheral nodule vasculature (Figures 1C, 1D, and S1D). These expression patterns for *LSH1* and *LSH2* are consistent with their cluster enrichment in recently obtained single-cell RNA-seq of 14-day-old nodules.[27] Consistent with their expression patterns in proliferating cells in nodule primordia and meristems, *LSH1* and *LSH2* expression was also observed in the proliferation zone of root meristems (Figure S1E). The observed gene expression patterns for *LSH1* and *LSH2* in early and mature nodules strongly overlapped with their protein localization patterns, assessed using GFP reporters translationally fused to the N terminus of *LSH1* and *LSH2* genomic sequences and expressed from their endogenous promoter and terminator sequences (Figure 1E).

LSH1 and *LSH2* have conserved floral development functions and negatively regulate lateral root emergence

To assess the roles of *LSH1* and *LSH2*, we identified loss-of-function mutants in *LSH1 (lsh1-1* and *lsh1-2)* and *LSH2 (lsh2-1)* and generated an *lsh1-1/lsh2-1* double mutant (Figure S2A). *lsh1*, but not *lsh2*, showed significantly altered shoot organ morphologies, including changes in petal shape and number and a reduction in stipule complexity (Figures 2A, 2B, S2B, and S2C; Table S1), revealing conserved floral functions across angiosperms.[26,28–30]

No effect for *LSH* has been reported in root system architecture, and we found no function for *LSH1* or *LSH2* in the promotion of lateral root development. Rather, we observed a slight increase in the number of lateral roots in *lsh1* and *lsh1/lsh2* (Figure S2D), suggesting that in *M. truncatula*, these genes may negatively regulate lateral root initiation. This was further corroborated by our observation that ectopic expression of either *LSH1* or *LSH2*, or both combined, resulted in a severe reduction in the number of emerged and elongated lateral roots (Figures 2C and S2E), with the majority of lateral root primordia in *LSH1*-overexpressing roots stalling/aborting at stages VI and

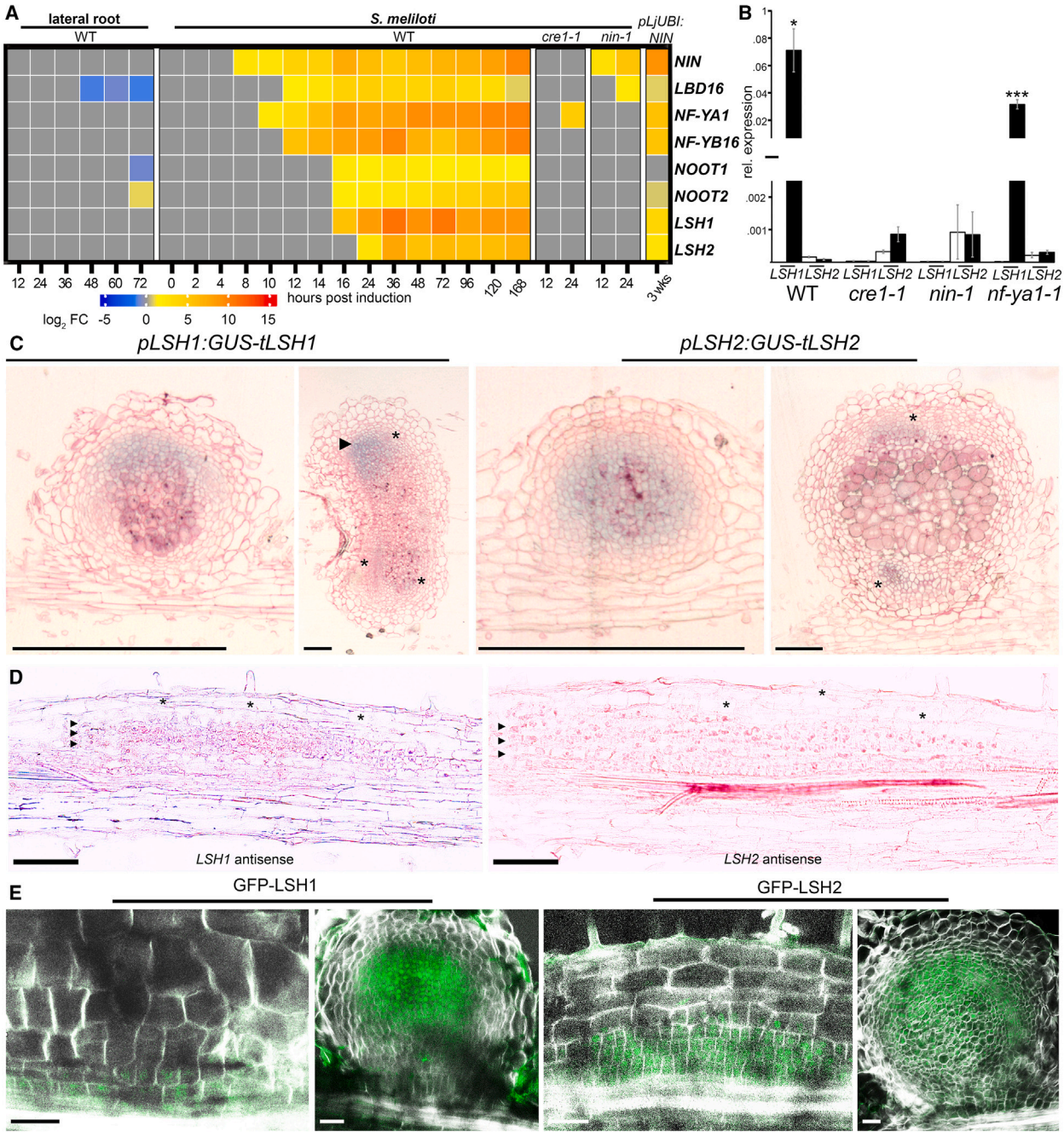

Figure 1. *LSH1* and *LSH2* are upregulated during early nodule organogenesis downstream of *NIN*

(A) Heatmap shows selected genes induced during lateral root and nodule development. Fold changes compared with controls are depicted in $\log_2$ scale $\geq \pm 0.585$ (raw fold change of 1.5), $p < 0.05$.

(B) Expression profiling on root segments treated with 100 nM 6-benzylaminopurine (BAP) for 24 h by quantitative reverse-transcription PCR (RT-qPCR) normalized to *HH3*. Statistical comparisons between mock (white bars) and BAP (black bars). Values are the mean ΔCt values of 3 biological replicates for *LSH1* and 2 for *LSH2* ± SEM (Student's t test; asterisks indicate statistical significance: *$p < 0.05$, **$p < 0.01$, ***$p < 0.001$).

(C) Promoter activity of *LSH1* and *LSH2* visualized by GUS (blue) (see also Figures S1D and S1E). Rhizobial-expressed *LacZ* is stained magenta. Ruthenium red demarks cell walls. Asterisks indicate expression in vascular bundles and arrows in the meristem. Scale bars, 500 μm.

(D) mRNA *in situ* hybridization on sections of WT roots 72 hpi with *LSH1* or *LSH2* antisense probes; arrows indicate *LSH1*/*LSH2* expression in dividing and newly divided nodule primordium cells, and asterisks indicate the lack of expression in the outer cortical and epidermal cell layers overlaying the nodule primordium. Scale bars, 100 μm.

(E) Optical sections of nodule primordia and mature nodules on hairy roots expressing *pLSH1:GFP-LSH1-t-LSH1* or *pLSH2:GFP-LSH2-t-LSH2* (in green) fluorescent brightener demarking cell walls (in white) and induced by spray inoculation with *Sm2011-mCherry* bacteria at 10 days post spray inoculation. Scale bars, 50 μm.

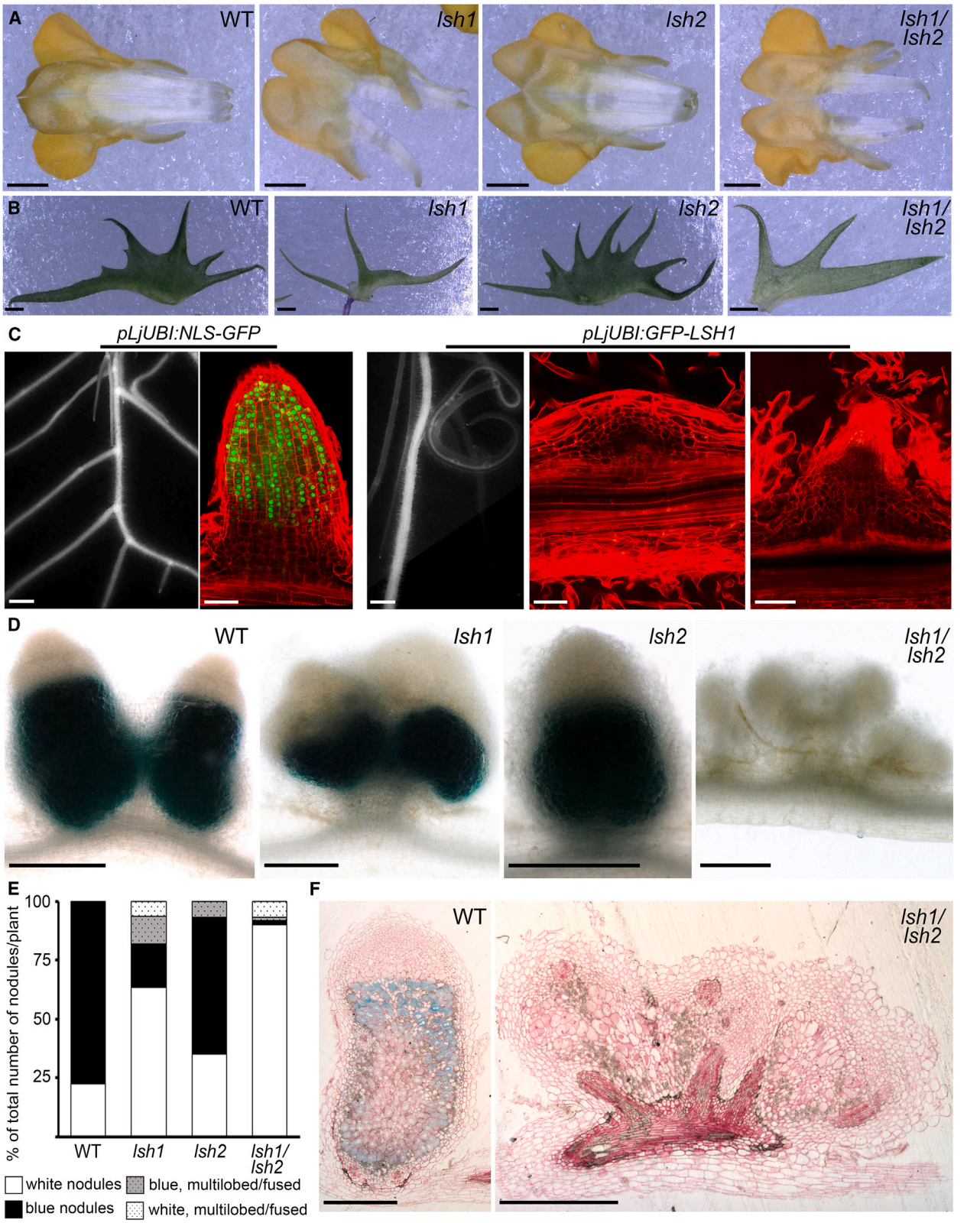

Figure 2. *LSH1/LSH2* are required for nodule development and N fixation

(A and B) Images of WT, *lsh1-2*, *lsh2-1*, and *lsh1-1/lsh2-1* dissected flower keels (A) and stipules (B); see also Figures S2B and S2C and Table S1. Scale bars, 500 μm.

(legend continued on next page)

VII[11] (Figures 2C, S2F, and S2G; Table S2). Together, these results show that *LSH1/LSH2* are negative regulators of lateral root development and positive regulators of floral organ development.

LSH1 and *LSH2* are required for nodule development and N fixation

For assessment of functions during nodulation, we inoculated plants with *Sinorhizobium meliloti* strain 2011 expressing *pNifH-GUS*, a bacterial promoter associated with the expression and activity of nitrogenase and used to approximate biological N fixation in nodules.[31] *lsh1* mutants showed a high frequency of white nodules, while the *lsh1/lsh2* double mutant developed almost exclusively white nodules, suggesting that N fixation was severely attenuated (Figures 2D–2F, S2H, and S2I). The reduction and absence of N fixation was confirmed in an acetylene reduction assay (Figure S2J). At 28 days post *S. meliloti* inoculation (dpi), *lsh1/lsh2* (Figure S2K) showed higher nodule frequency, a phenomenon frequently observed in fix$^-$ mutants.[31] Nodule morphology was significantly altered in *lsh1* and *lsh1/lsh2*, with frequent multilobed and fused nodules (Figures 2D–2F, S2H, and S2I). Nodule sections revealed a severe reduction in the number of cells with intracellular bacterial colonization in *lsh1/lsh2* nodules, but no obvious defects were observed in bacteroid differentiation in the few cells that possessed intracellular colonization (Figure S3A).

LSH genes are required for the development of nodule primordia that can support bacterial colonization

To further investigate the cause of this severe reduction in rhizobial colonization, we assessed the progression of rhizobial infection and early nodule primordium development. In WT, the progression of rhizobial infection threads through the epidermis and cortex was temporally and spatially coordinated with the development of the nodule primordium (Figures 3A, 3B, S6A, and S6B). We observed nodule primordium initiation and early establishment of epidermal infection threads in *lsh1* and *lsh1/lsh2*; however, the progression of infection threads through the mid-cortex and subsequent internal colonization of primordium cells were severely impaired (Figures 3A, 3B, S6A, and S6B). This resulted in a high proportion of *lsh1* and *lsh1/lsh2* nodules that were partially or completely uncolonized.

A recent study highlighted the importance of reduced mitotic potential and the modulation of the G2/M cell-cycle transition as a key context for successful transcellular passage of cortical cells by rhizobial infection threads overlaying the developing nodule primordium.[32] We used the dual-color H3.1/H3.3 histone reporter to assess the cellular state of cortical cells during rhizobial infection. We observed that the histone H3.1 eviction and enlargement of nuclei, which coincide with cortical infection thread progression, were comparable between *lsh1/lsh2* and WT (Figure 3C). This demonstrates that cortical cells associated with infection progression develop normally in *lsh1/lsh2* and are consistent with infection-associated gene expression also appearing relatively unaffected in *lsh1/lsh2* (discussed later). Coupled with the fact that *LSH1/LSH2* expression is restricted to the newly divided cells in the nodule primordium (Figures 1D and 1E), this strongly implies that *LSH1/LSH2* are not directly required for the genetic program associated with infection thread initiation and progression. Rather, we propose that the limitations to infection thread progression in *lsh1/lsh2* are the result, directly or indirectly, of *LSH1/LSH2* function in early nodule morphogenesis and subsequent host cell fate acquisition and maintenance.

In support of this hypothesis, while we found few differences between WT and *lsh1/lsh2* at 24 h (Figure S3B), when early cell division is initiated by *LBD16*,[9] we observed a severe reduction in cell-cycle activity in *lsh1/lsh2* primordia at 72 hpi, compared with WT: cells in the mid-cortex of WT primordia had undergone periclinal divisions, generating cell layers that form the interface for the first intracellular bacterial colonization of the nodule primordium, whereas these cortical-derived cell layers were severely reduced or absent in *lsh1/lsh2* (Figures 3D and S3C). Concomitant to this reduction in cell-cycle activity in the cortex, we observed continued cell-cycle activity at the nodule initiation site in the inner tissue layers of the *lsh1/lsh2* mutant, suggesting that control of these cellular processes is at least in part independent and genetically separable from the function of *LSH1/LSH2*. Consequently, periclinal cell divisions originating from the inner tissue layers at the base of the nodule appeared to contribute substantially higher numbers of cells to the emerging *lsh1/lsh2* nodule in comparison with WT (Figures 3D, S3C, and S3D), coincident with an increased number of cells of high nuclear H3.1 content (Figure S3D). The cellular origin of the structures that emerge in *lsh1/lsh2* is much more closely related to lateral roots than to nodules,[9,11,12] and we propose it is this lack of appropriate mid-cortical cell division that leads to the severe reduction of bacterial infection.

LSH1 and *LSH2* function as key transcriptional regulators in nodulation

To understand how *LSH* function is driving this nodule-specific cell division and associated nodule identity, we made use of our extensive transcriptomic profile during early and late nodule development (Figure 4A).[9] We performed RNA-seq on rhizobial spot-inoculated root sections of *lsh1* and *lsh1/lsh2*, compared with WT, at 24 and 72 hpi (Figures 3D, S3B, and S3C). Surprisingly, this revealed that >90% of rhizobial-responsive genes in WT were not differentially expressed in the *lsh1/lsh2* mutant (Figure 4A), with many of these gene expression differences

(C) Whole-mount images of hairy roots expressing *pLjUBI:NLS-GFP* (control) and *pLjUBI:GFP-LSH1*. Epifluorescence images: scale bars, 1 mm; confocal images: 5-ethynyl-2′-deoxyuridine (EdU)-labeled nuclei indicating DNA replication in green and propidium iodide-stained cell walls in red demarking cell geometry. Scale bars, 50 μm (see also Figures S2E–S2G and Table S2).

(D) Whole-mount images of WT, *lsh1-1*, *lsh2-1*, and *lsh1-1/lsh2-1* nodules 28 days post *S. meliloti* inoculation. GUS staining (blue) indicates the expression of the bacterial *pNifH* promoter. Scale bars, 500 μm.

(E) Distribution of different nodule morphologies depicted as percentage of total nodule number per plant in WT and *lsh1-1* (n = 15), *lsh2-1* (n = 14), and *lsh1-1/lsh2-1* (n = 13) (see also Figures S2H–S2K).

(F) Sections of 28-day-old nodules in WT, *lsh1-1*, and *lsh1-1/lsh2-1*, *pNifH:GUS* expression (blue), ruthenium red demarks cell walls. Scale bars, 500 μm.

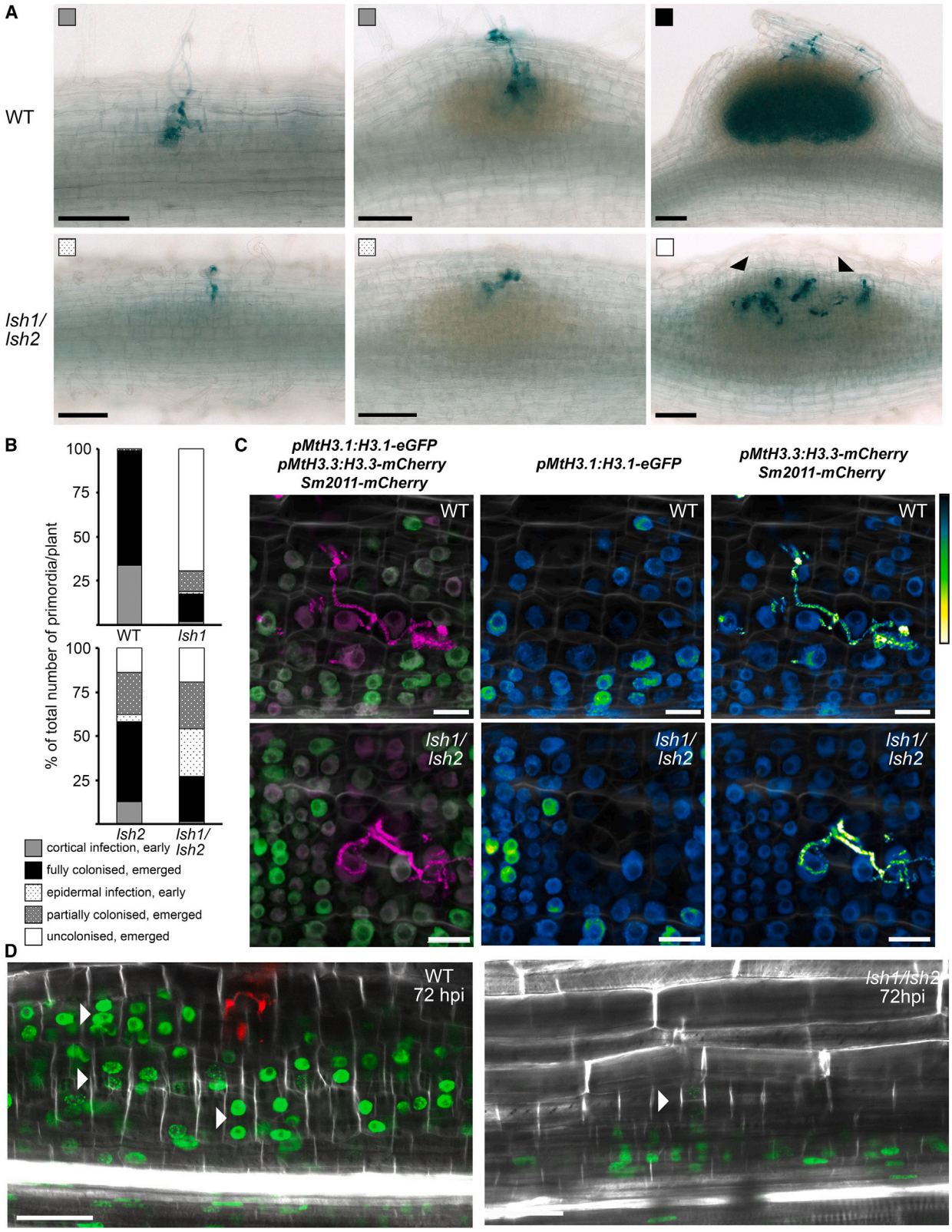

(legend on next page)

already present at 24 hpi. This severe reduction in the overall transcriptional response to rhizobial inoculation emphasizes the major regulatory contribution of *LSH1/LSH2* to nodulation.

To identify the putative direct LSH targets, we undertook ChIP-seq on roots ectopically expressing a *GFP-LSH1* translational fusion (*pLjUBI:GFP-LSH1*; using *pLjUBI-NLS-GFP* as control). In addition, we characterized the transcriptional effects of combined *LSH1/LSH2* overexpression (*LSH1+LSH2* OE) under non-symbiotic conditions (Figures 2C, S2E, S2F, and S4A). These analyses revealed significant LSH1 DNA-binding sites for 3,714 genes that were previously identified to be differentially expressed in response to rhizobial infection in WT,[9] suggesting that 18% (3,714/20,719) of the total number of nodulation-associated differentially expressed genes (DEGs) are under direct control of LSH1 (Figure 4A). We clustered the time-resolved nodule-associated DEGs (20,719) based on their $\log_2$ fold changes into 17 clusters and assessed the representation of the 2,552 LSH1-ChIP-seq and *LSH1/LSH2* OE-responsive targets (Figure 4A; Data S1). Putative direct *LSH*-responsive targets were equally represented in clusters of upregulated and downregulated genes, suggesting that *LSH* can act as both activators and repressors. A high representation ($\geq$the average of 18%) of LSH1-ChIP-seq and *LSH1/LSH2* OE-responsive targets was found in the clusters of genes that were induced during the 16–72 hpi-time points at the stages of cell proliferation and onset of differentiation, further corroborating a direct regulatory function during nodule organogenesis for *LSH1/LSH2*. By contrast, representation was lower ($\leq$12%) in clusters of genes that peaked in their differential expression very early or very late, indicating that *LSH1/LSH2* play a less significant role in early establishment of rhizobial infection and nodule initiation or in the maintenance of N fixation (Figure 4A; Data S2B and S2C). Consistently, marker genes for symbiosis signaling and early infection, such as *EARLY NODULIN 11* (*ENOD11*) and *Rhizobium-directed Polar Growth* (*RPG*), were not directly targeted by *LSH1/LSH2* and still expressed in *lsh1/lsh2*. In contrast, genes associated with infection progression and N fixation, such as *VAPYRIN* (*VPY*) and LEGHEMOGLOBINs (*LB1/LB2*), were indirectly affected in the *lsh1/lsh2* mutant (Figure S4B).

The 3,714 nodulation-associated LSH1-ChIP-seq targets were clustered by their $\log_2$-fold expression changes upon rhizobial spot inoculation. The Gene Ontology (GO) enrichment analysis on the clusters revealed an enrichment of GO terms related to cell division and shoot development, including auxin and cytokinin biosynthesis and signaling, in upregulated genes and response to biotic and abiotic stresses in downregulated genes (Figure S4C; Data S2B and S2C). This included several key components of the auxin-cytokinin crosstalk, such as *STY-I* transcription factors promoting local auxin biosynthesis in nodulation; *PIN-FORMED 1* (*PIN1*) and *PINOID* (*PID*) genes; as well as genes involved in the biosynthesis, catabolism, and transport of cytokinin, which include *ISOPENTENYL TRANSFERASE 1* (*IPT1*), members of the *LONELY GUY* (*LOG*), *CYTOKININ OXIDASE* (*CKX*) gene families, the G subfamily of *ATP BINDING CASSETTE* transporters (*ABCG*), and cytokinin signaling genes such as *CRE1* and the response regulators *RR2* and *RR8* (Figures 4C and 4D).[20,34–38] Cell-cycle regulators were also directly controlled by LSH1, including D-type cyclin *CYCD3;1* and mitotic B-type cyclin *CYCB1;2*, while the endoreduplication regulator *CSS52B* was indirectly dependent on *LSH1/LSH2*.[39,40] Consistent with the suppression of lateral root development, we found the *PLETHORA* root meristem regulators (*PLT1* and *PLT2*)[41–43] to be under direct repression by *LSH1/LSH2* (Figure 4E).

Several LSH1-ChIP-seq targets and *LSH1/LSH2*-responsive genes have previously been annotated to function as meristem and growth regulators in the shoot, highlighting the pleiotropic function of *LSH* transcription factors. This includes the *Medicago* orthologs of the transcriptional co-activators *BOP* and *MtNOOT1/MtNOOT2*, two well-characterized nodule organ identity genes.[14,15,44]

LSH1 and *LSH2* directly regulate *NOOT1/NOOT2* that function in the same pathway during nodule organogenesis

NOOT1/NOOT2 are important regulators of nodule identity: in their absence, nodules initiate but revert to a lateral root identity, suggesting that *NOOTs* are key maintainers of the nodulation program.[14,15] Our observations that *NOOTs* are direct targets of *LSH1/LSH2* suggest that the control of these transcription factors may be a key feature of *LSH* functionality. Promoter-GUS analysis of *pNOOT1:GUS-tNOOT1* and *pNOOT2:GUS-tNOOT2* in WT and *lsh1/lsh2* revealed that *NOOT* gene expression in nodule primordia was *LSH* dependent, although still present at the base of the developing *lsh1/lsh2* nodule (Figure 5A). Expression profiling of spot-inoculated root sections of *noot1/noot2* revealed that loss of *NOOT1/NOOT2* affects a comparatively smaller subset of the rhizobial-induced genes than the loss of *LSH1/LSH2* ($\leq$60% of rhizobial-responsive genes in the WT at

Figure 3. *LSH* genes are required for the development of nodule primordia that can support bacterial colonization

(A) Images of WT and *lsh1/lsh2* nodule primordia at different developmental stages, first initial divisions (left), multilayered (middle), and emerged primordia (right) observed 7 days post spray inoculation with rhizobial bacteria expressing *LacZ* (blue stain). Black arrowheads indicate infection threads that are restricted in their progression into the inner root tissue layers. Squares relate to the legend in (B). Scale bars, 500 μm.

(B) Distribution of bacterial colonization phenotypes observed in WT, *lsh1*, *lsh2*, and *lsh1/lsh2* at 7 dpi depicted as percentage of the total primordia number per plant, WT (n = 30), *lsh1, lsh2* (n = 33), *lsh1/lsh2* (n = 32).

(C) Confocal images of whole-mount transgenic roots co-expressing *H3.1-eGFP* (green) and *H3.3-mCherry* (magenta) in WT (n = 7 independent hairy root systems) and *lsh1/lsh2* (n = 10 independent hairy root systems) inoculated with *Sm2011-mCherry* (magenta) at 6 dpi (left). Images are maximum intensity projections (eGFP/mCherry signal either depicted in green/magenta (left) or in the green fire blue color range, blue to yellow indicating min to max fluorescence levels (middle and right) and calcofluor demarking cell walls (white). Scale bars, 20 μm.

(D) Optical sections of WT and *lsh1/lsh2* roots 24 and 72 hpi with *S. meliloti* (n > 30 per genotype and time point); see also Figures S3B and S3C and Table S3. At 72 hpi, *Sm2011-mCherry* bacteria in red, cell walls in white (fluorescent brightener), and EdU-labeled nuclei indicating DNA replication in green. White arrowheads indicate periclinal cell divisions. Scale bars, 50 μm.

See also Figure S6.

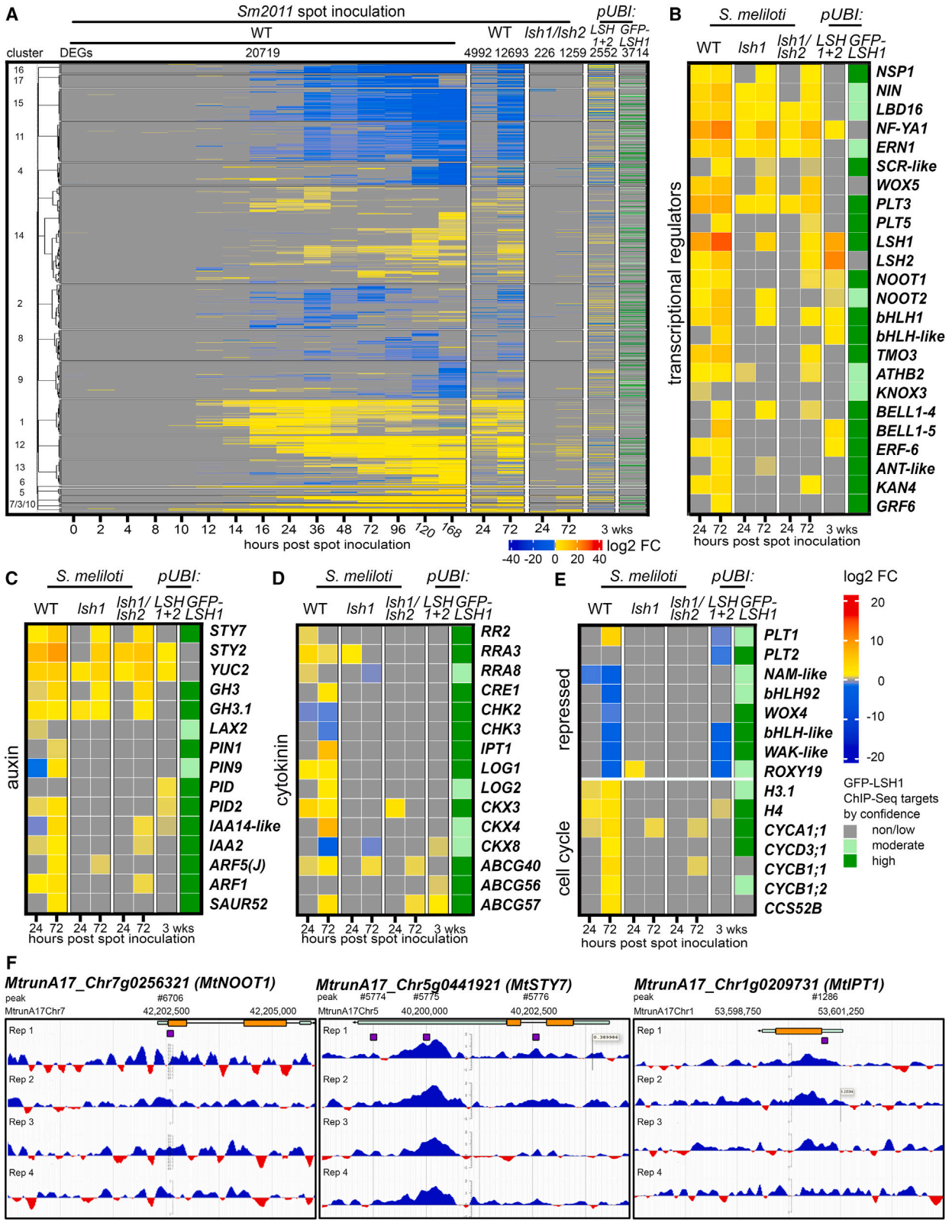

Figure 4. *LSH1* and *LSH2* function as key transcriptional regulators in nodulation

(A) Heatmaps of all DEGs in response to *S. meliloti* spot inoculation in WT clustered according to their expression patterns into 17 clusters,[9] aligned with heatmaps of DEGs in WT (*R108*), *lsh1*, and *lsh1/lsh2* at 24 and 72 hpi, and in response to combined ectopic expression of *LSH1/LSH2* (*pLjUBI:LSH1+LSH2*) compared with

(legend continued on next page)

24 and 72 hpi [Figures 4A and 5B]). Interestingly, there was a complete overlap (≥99.9%) between the genes that were affected in their response to rhizobial spot inoculation in the *noot1/noot2* and in the *lsh1/lsh2* mutants and a large overlap between the expression profiles of the OE lines, suggesting that the effect on gene expression caused by gain and loss of *NOOT1/NOOT2* is embedded in the *LSH1/LSH2* function (Figures 5C and S5B). Gain or loss of *NOOT1/NOOT2* has no effect on *LSH1* or *LSH2* expression (Figure S5A), suggesting that *NOOT1/NOOT2* function downstream of *LSH1/LSH2*.

Comparing the early nodule developmental phenotypes of *lsh1/lsh2* and *noot1/noot2* revealed clear differences in the functions of these genes: whereas *lsh1/lsh2* show reductions in the periclinal cell divisions of the mid-cortex, *noot1/noot2* primordia show cell-cycle activities comparable with or greater than that of WT (Figures 3C, 6A, and 6B) and WT rhizobial infection at these early time points (Figure S6A), as previously reported.[15] However, at later stages of nodule development, *noot1/noot2* showed similar defects to *lsh1/lsh2*, resulting in a large proportion of partially or completely uncolonized nodules (Figures 3A, 3B, and S6A–S6C).

An *lsh1/noot1* double mutant recapitulated the phenotype of the *lsh1/lsh2* double mutant (Figures 6A, 6B, and S6A–S6C), highlighting the genetic interactions between these two classes of genes. The phenotypic resemblance between the *lsh1/noot1* and *lsh1/lsh2* mutants was present also at early time points, with infection defects and reductions in periclinal cell divisions in the mid-cortex of the root in both *lsh1/noot1* and *lsh1/lsh2* mutants (Figures 3D, 6C, S6A, and S6B). A striking aspect of the *noot* mutant phenotype is the emergence of lateral roots from the tips of nodules.[14,15] We observed this phenotype in *lsh1/lsh2* but at a lower frequency to that observed in *noot1/noot2* (Figures 6A, 6B, and S6C), consistent with the loss of repression of the root meristem genes *PLT1/PLT2* in both *lsh1/lsh2* and *noot1/noot2* (Figures 4E and S5A). Despite the genetic interactions between *NOOT* and *LSH*, the ectopic expression of *NOOT1/NOOT2* was not sufficient to rescue *lsh1/lsh2* ($n > 5$). Studies in other plant species have shown direct protein interactions between *LSH* and *BOP* genes, the orthologs of *NOOT1/NOOT2*[26,45]; however, we have been unable to find any evidence for direct interactions between LSH1/LSH2 and NOOT1/NOOT2, using the bimolecular fluorescence complementation (BiFC) assay in *M. truncatula* roots. We conclude that *LSH1/LSH2* directly control the expression of *NOOT1/NOOT2* in the nodule primordium, which in part explains the later developmental functions of *LSH*, but not the early specification of mid-cortex cell divisions, with *NOOTs* maintaining the nodule identity preset by *LSH1/LSH2*.

LSH1 and *LSH2* partly function through the cortical activation of *NF-YA1*

In addition to *NOOTs, NF-YA1* has also been shown to function in nodule development,[10,12,18–20] and while we did not find *NF-YA1* to be a direct target of LSH1, we observed a partial dependence on *LSH1/LSH2* for appropriate *NF-YA1* expression during nodulation and activation of *NF-YA1* as a function of *LSH1/LSH2* OE (Figure 4B). Comparing *lsh1/lsh2* and *nf-ya1* mutant phenotypes, we found many similarities, including an increased ratio of aborted cortical infection threads and a reduction in cell divisions and cell layers in the nodule primordium (Figures 2D–2F, 3A–3D, and S7A–S7G). Consistently, comparison of rhizobial-responsive DEGs in *lsh1/lsh2* and *nf-ya1* and of *LSH1* and *NF-YA1* OE-responsive DEGs (Figures 7C, S7H, and S7I; Data S1) revealed convergences in their gene regulation in genes associated with local biosynthesis, transport, and conjugation of auxin and in cytokinin metabolism and signaling.[19,20]

Promoter-GUS analysis of *pNF-YA1:GUS-tNF-YA1* showed expression in the inner tissue layers at the base of developing nodules and in nodule primordia (Figure 7A), with *NF-YA1* expression in the cortex-derived cells of the nodule primordium being *LSH1/LSH2* dependent (Figure 7A). The reduced cortical expression of *NF-YA1* might at least in part explain the nodulation defects in *lsh1/lsh2*. To test this, we ectopically expressed *NF-YA1* under the constitutive *LjUBI* promoter or under both the *pLSH1* and *pLSH2* promoters in *lsh1/lsh2* roots. Both modes of *NF-YA1* expression resulted in a partial rescue of *lsh1/lsh2*, leading to 25% of nodules with functional N fixation, based on *pNifH-GUS* (Figure 7B; Table S4), revealing that *NF-YA1* regulation by *LSH* is a key aspect of *LSH* functionality, leading to N-fixing nodules.

NF-YA1 is one of the earliest induced transcription factors in response to rhizobial recognition and plays a role in the establishment of bacterial infection.[9,10,46] This is an important differentiator between *LSH* and *NF-YA1* functionality, and consistently genes involved in early stages of rhizobial infection such as *RPG* were affected and responsive to loss and/or gain of *NF-YA1*, but not to *LSH1/LSH2* (Figure 7C; Data S1). While *NF-YA1* expression is in part controlled by *LSH1/LSH2*, we saw no evidence for the converse (Figures 1B and 7C), revealing that *NF-YA1* functions downstream of *LSH1/LSH2*.

DISCUSSION

The initiation of symbiotic root nodules and lateral roots converges on the upregulation of the transcription factor *LBD16*, which allows for the initiation of cell divisions in the inner root

empty vector in 3-week-old WT hairy roots. Expression levels are depicted as $\log_2$ fold changes ≥ ±0.585 (raw fold change of 1.5), $p < 0.05$. Absolute numbers indicate the number of DEGs in each genotype. Dark green, light green, and gray coloring in the far right column depict confidence levels of LSH1 DNA-binding sites associated with DEGs detected in ≥3/4, 2/4, and ≤1/4 biological replicates comparing pull-downs of GFP-bound DNA fragments in *pLjUBI:GFP-LSH1* compared with *pLjUBI:NLS-GFP*, respectively.

(B–E) Heatmaps showing expression levels of selected functional groups of DEGs in WT, *lsh1*, and *lsh1/lsh2* root sections at 24 and 72 hpi and in response to combined ectopic expression of *LSH1/LSH2* (*pLjUBI:LSH1+LSH2*) compared with empty vector in 3-week-old WT hairy roots, alongside LSH1 DNA-binding sites (far right column) according to their confidence levels. Fold changes compared with controls are depicted in $\log_2$ scale ≥ ±0.585 (raw fold change of 1.5), $p < 0.05$. Related to Figures 5B, 7C, S4A–S4C, and S5A. See also Data S1, S2B, and S2C.

(F) Representative ChIP-seq peaks in 4 biological replicates comparing pull-downs of GFP-bound DNA fragments in *pLjUBI:GFP-LSH1* compared with *pLjUBI:NLS-GFP*, visualized in the *MtrunA17r5.0-ANR* Genome Browser.[33] Blue peaks denote regions where the immunoprecipitated samples show an increased number of mapped reads, compared with the control samples, and the red peaks denote the opposite. The purple rectangles indicate high-confidence DNA-binding sites (found in ≥3/4 biological replicates).

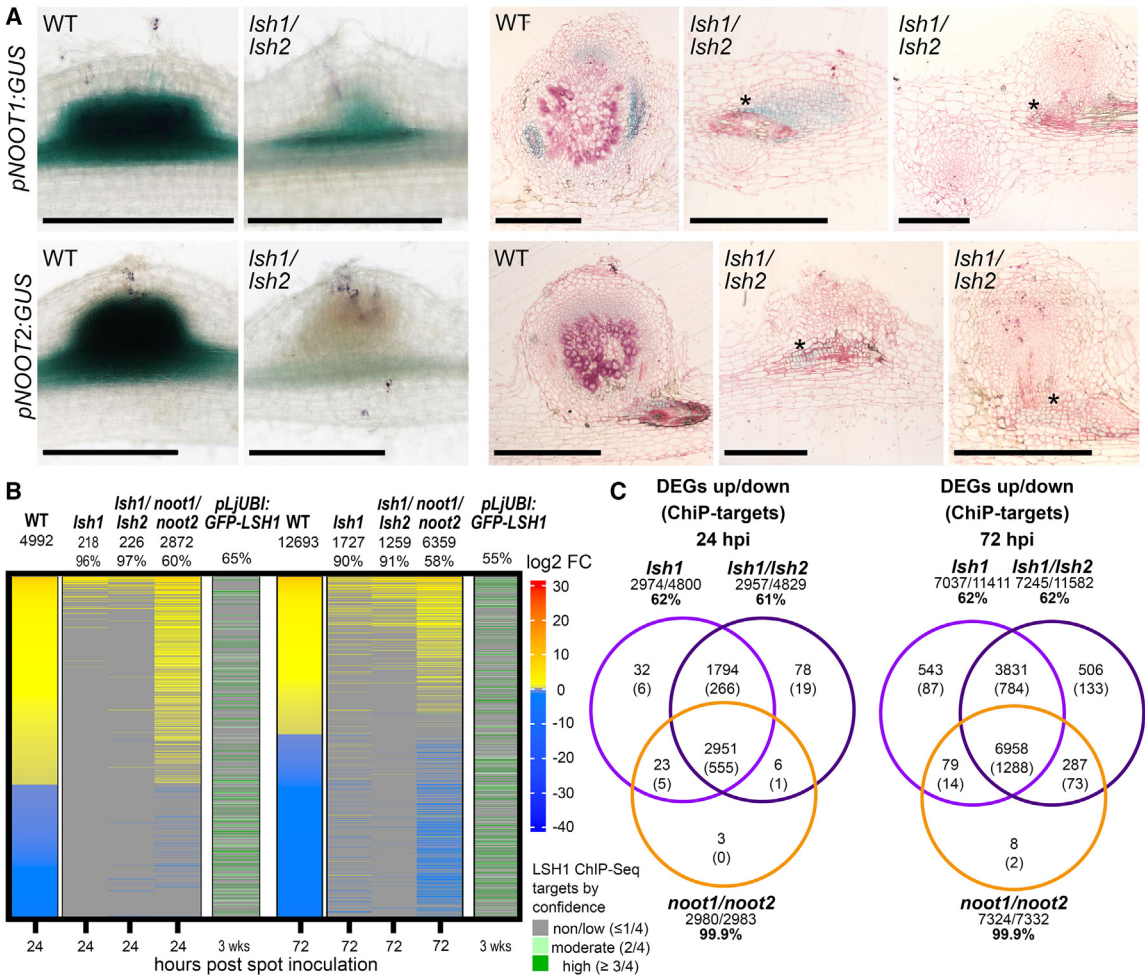

Figure 5. *LSH1/LSH2* promote the expression of and act together with *NOOT1/NOOT2*

(A) Expression patterns of *NOOT1* and *NOOT2* in WT and *lsh1/lsh2* nodules, visualized by GUS staining (blue) in whole-mount images (left) and nodule sections (right). Rhizobial-expressed *LacZ* is stained magenta. Ruthenium red demarks cell walls in sections. Black asterisks indicate vascular expression at the nodule base. Scale bars, 500 μm.

(B) Related to Figures 4A, S5A, and S5B; see also Data S1, S2B, and S2C. Heatmaps of all DEGs in WT, *lsh1*, *lsh1/lsh2*, and *noot1/noot2* at 24 and 72 hpi. Expression levels are depicted as $\log_2$ fold changes ≥ ±0.585 (raw fold change of 1.5), $p < 0.05$. LSH1 DNA-binding sites associated with rhizobial-responsive DEGs are depicted in dark green: high confidence, light green: moderate confidence, or gray: low/no confidence. To compare the overall transcriptional response to *S. meliloti* spot inoculation between WT and the mutants, we sorted all DEGs from the highest positive to the highest negative $\log_2$ fold change values. Absolute numbers indicate responsive DEGs, and percentages indicate the proportion of DEGs in WT that are not differentially expressed in the mutants and therefore affected by loss of *LSH1*, *LSH1/LSH2*, and *NOOT1/NOOT2*.

(C) Comparisons of all DEGs affected in *lsh1* (light purple), *lsh1/lsh2* (dark purple), and *noot1/noot2* (orange) upregulated and downregulated at 24 and 72 hpi. Numbers in brackets refer to high and moderate LSH1 ChIP-seq targets. Genes with $\log_2$ fold changes ≥ ±0.585 (raw fold change of 1.5), $p < 0.05$ were included in this analysis.

See also Figures S5 and S6 and Table S4.

tissues.[9,10] Despite these similarities during the initiation stages, the development of nodules and lateral roots diverges, with nodules differentiating into organs that can intracellularly accommodate rhizobial bacteria and provide the environment for biological N fixation. Here, we show that nodule-specific development is to a large extent directly orchestrated by *LSH1/LSH2*, two members of the *LSH* transcription factor family with previously reported pleiotropic functions in shoot development.[26,29,45] Like *LBD16*, *LSH1/LSH2* are controlled by *NIN* downstream of cytokinin signaling, suggesting parallel activation of two conserved programs. *LBD16* and *LSH1/LSH2* appear to have spatially and temporally separable roles: *LBD16* allows the initial activation of cell divisions in the inner tissue layers, with the resultant divisions and developmental outcomes being closely related to the initiation of lateral roots. In contrast, *LSH1/LSH2* control a very specific set of cell divisions with distinct identity and fate trajectory in the mid-cortex of the root, which are unique to nodules and are directly associated with the creation of cells able to accommodate N-fixing bacteria.[12] *LSH1/LSH2* promote the cortex-specific expression of the previously identified nodule regulators *NOOT1/NOOT2* and *NF-YA1* that converge and synergize in their regulatory functions

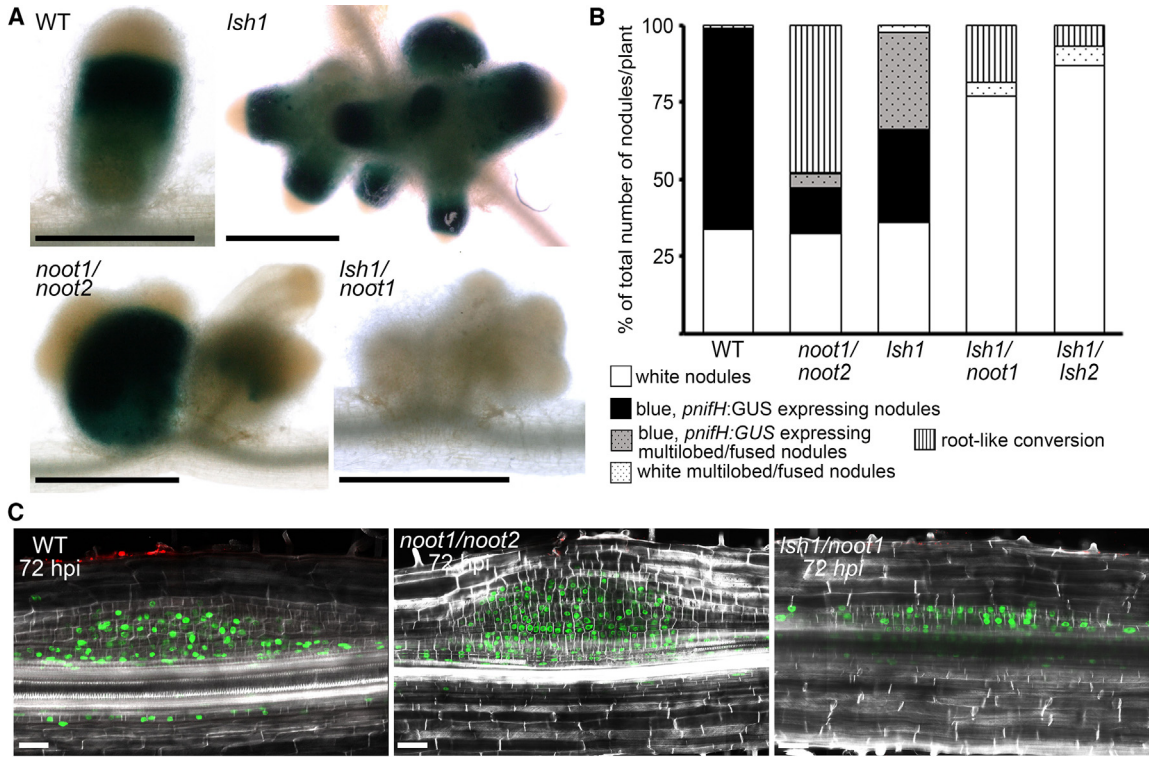

Figure 6. *LSH1/LSH2* and *NOOT1/NOOT2* function synergistically to confer nodule organ identity

(A) Whole-mount images of WT, *lsh1*, *noot1/noot2*, and *lsh1/noot1* nodules at 21 days post *S. meliloti* inoculation. GUS staining (blue) indicates the expression of the bacterial *pNifH*. Scale bars, 500 μm.

(B) Distribution of different nodule morphologies and N fixation (*pnifH:GUS* staining) at 21 dpi depicted as percentage of the total nodule number per plant, WT (n = 37), *noot1/noot2* (n = 44), *lsh1* (n = 33), *lsh1/noot1* (n = 35), *lsh1/lsh2* (n = 40) (see also Figure S6C).

(C) Optical sections of WT, *noot1/noot2*, and *lsh1/noot1* root sections 72 hpi (n > 15 per genotype). *Sm2011-mCherry* bacteria in red, cell walls in white (fluorescent brightener), and EdU-labeled nuclei indicating DNA replication in green. Scale bars, 50 μm. For comparison with *lsh1/lsh2*, see also Figures 3D and S3C and Table S3).

See also Figures S5 and S6.

in the modulation, amplification, and maintenance of the auxin-cytokinin crosstalk, a key feature and differentiator between lateral root and nodule development.[15,20]

Legumes appear unique in their ability to respond to cytokinin with the promotion of mitotic cell divisions in the root, and this ability is the function of NIN promotion of *LBD16*, which upregulates local auxin biosynthesis.[7,9,47] Crosstalk between polar auxin transport and cytokinin signaling has previously been shown to determine cell division patterns and the onset of cell differentiation in the transition zone of the root and during lateral root development.[48–52] Equally, the maintenance of cytokinin homeostasis and cytokinin signaling have been shown to play vital roles in promoting nodule organogenesis and endosymbiotic host cell specification in legumes.[8,34,39,53,54] Critically, the impacts of cytokinin are opposing in lateral root and nodule development.[8,47,55] We demonstrate that the promotion of cytokinin signaling during nodulation is sustained by *LSH1/LSH2* via direct and indirect (via *NOOTs* and *NF-YA1*) mechanisms, providing a means for divergence between lateral roots and symbiotic nodules. The direct and indirect (via *NOOTs*) transcriptional repression of the lateral root program during nodulation, via repression of the root meristem regulators *PLT1/PLT2*, provides another means to modulate the auxin/cytokinin balance.[42,43,52] Such differentiation in development is critical, since lateral roots and nodules initiate comparably[9–12] and only later diverge in their development.

The severe nodulation defects caused by loss of *LSH1/LSH2* can be partially explained by *LSH1/LSH2* regulation of *NF-YA1*. Previously, *NF-YA1* has been characterized as a direct downstream target of *NIN* and shown to be involved in nodule initiation and the progression of bacterial infection.[10,23,46] Based on our results, we propose that *LSH1/LSH2* promote *NF-YA1* expression specifically in the newly divided cells derived from the mid-cortical cell layers associated with the specification of the nodule primordium. Our data point toward an indirect regulation by *LSH1/LSH2*, perhaps via promotion of cytokinin and *NIN* in the cortex, subsequent and in parallel to its reported direct upregulation by *NIN* at the base of the developing nodule.[10,56] Recent findings that implicate *NF-YA1* in infection competence via post-replicative cell-cycle regulation at the G2/M phase transition and promotion of endoreduplication provide an interesting mechanism by which our observed partial rescue of the *lsh1/lsh2* mutant by ectopic *NF-YA1* expression may be explained,[32] since endosymbiotic host cell colonization is facilitated by the switch from mitotic cell proliferation to endoreduplication.[32,39,40,57]

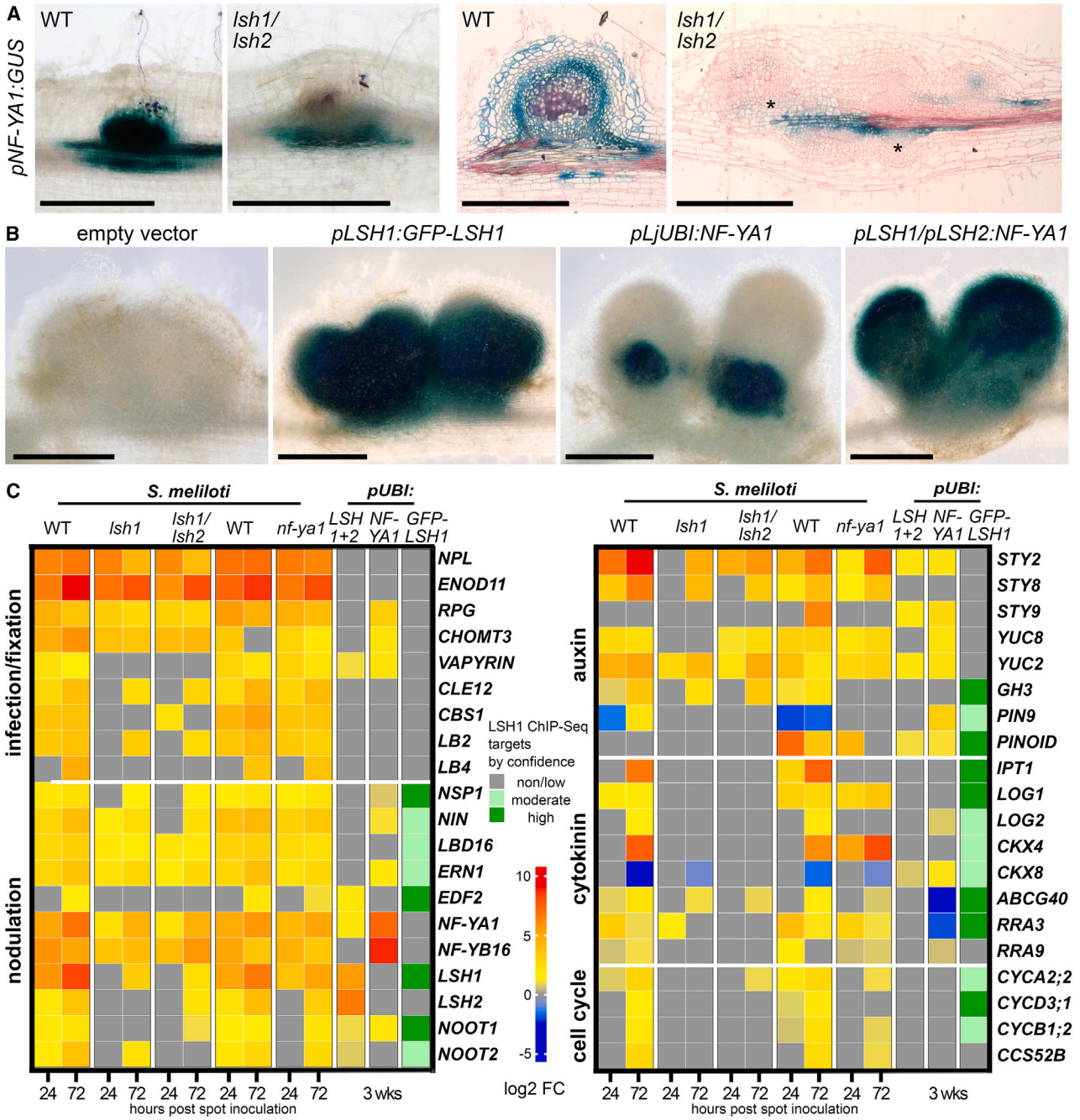

Figure 7. *LSH1/LSH2* partly function through the cortical activation of *NF-YA1*

(A) Expression pattern of *NF-YA1* in WT and *lsh1/lsh2*, visualized by GUS staining (blue) in whole-mount images (left) and nodule sections (right). Rhizobial-expressed *LacZ* is stained magenta. Ruthenium red demarks cell walls in sections. Black asterisks indicate vascular expression restricted at the nodule base. Scale bars, 500 μm.

(B) Whole-mount images of nodules on hairy roots of *lsh1/lsh2* plants transformed with empty vector control, *pLSH1:LSH1*, *pLjUBI:NF-YA1*, and combined *pLSH1:NF-YA1/pLSH2:NF-YA1* at 28 dpi with *S. meliloti* expressing *pNifH:GUS*. GUS staining (blue) indicates the expression of the bacterial *pNifH* promoter (see also Table S4). Scale bars, 500 μm.

(C) Heatmap of selected functional groups of DEGs in WT, *lsh1*, *lsh1/lsh2*, and *nf-ya1* at 24 and 72 hpi and in response to combined ectopic expression of *LSH1/LSH2* (*pLjUBI:LSH1/LSH2*) or *NF-YA1* (*pLjUBI:NF-YA1*) compared with empty vector control in 3-week-old WT hairy roots under non-symbiotic conditions. Fold changes compared with controls are depicted in $\log_2$ scale $\geq \pm 0.585$ (raw fold change of 1.5), $p < 0.05$. LSH1 DNA-binding sites associated with DEGs are depicted in dark green: high confidence, light green: moderate confidence, or gray: low/no confidence.

See also Figure S7 and Data S1, S2B, and S2C.

A key feature of nodules is their ability to intracellularly accommodate N-fixing bacteria. However, the detailed regulatory mechanisms remain unclear. In the shoot, *LSH* genes have been shown to regulate the activity of meristems and the growth of lateral organs with a proposed function in promoting the appropriate amount of undifferentiated cells that can serve as a canvas for the differentiation of complex organs with intricate features and functions.[26,29,30] This is exemplified by their role in the development of indeterminate compound inflorescences[29,30] and the development of stipules with complex serrations, as demonstrated here. We propose that these previously described shoot functions of *LSH* and its co-recruited shoot-expressed regulatory subnetwork are of relevance during nodule development, where early cell patterning processes need to be spatially and temporally coordinated with the arrival of the colonizing bacteria. Perhaps it is the maintenance of cells in an undifferentiated state, through the promotion of *LSH1/LSH2* expression, that allows their extensive colonization by bacteria, or alternatively, perhaps it is the pausing of cellular differentiation to align with the timing of bacterial infection that is so critical. Further work is clearly required to understand the process of bacterial infection and accommodation in nodules: the transcriptional network controlled by *LSH1/LSH2* provides an excellent launchpad for these studies.

Here, we propose a model for specific nodule development: cytokinin activation of *NIN* expression initiates the nodule primordium through induction of *LBD16*, which activates local auxin biosynthesis to drive cell divisions in a manner comparable to lateral root initiation. In parallel, *NIN* activates the expression of *LSH1/LSH2* to promote cell divisions specifically in the mid-cortex and control and maintain nodule organ identity, in part through the transcriptional promotion of *NOOT1/NOOT2* and *NF-YA1*, as well as further promoting auxin-cytokinin levels and directly suppressing the lateral root developmental program. *LSH1/LSH2* drive cell divisions that provide cells able to accommodate N-fixing bacteria, possibly through a combination of promoting endoreduplication and maintaining the cells in an undifferentiated state, at least until the arrival of the infection threads.

While nodules are unique structures associated with symbiotic bacterial N fixation, we have yet to see any evidence for *de novo* gene evolution associated with the emergence of nodulation. Rather, we find evidence for the re-networking of preexisting developmental pathways, facilitating the emergence of this novel form of root development. The neo-functionalization of the nodule-specific transcription factor *NIN* and the associated evolution of *cis*-regulatory DNA-binding sites in the promoter regions of its downstream targets led to the recruitment of a lateral root organ initiation program into the symbiotic interaction with rhizobial bacteria.[9,10,13,58] Similarly, we hypothesize that further neo-functionalization of *NIN* provided the opportunity for recruiting a growth-regulatory network with pleiotropic functions in the shoot into the symbiotic root context, thereby promoting the expansion and diversification of the regulatory function of *LSH1/LSH2* and their associated downstream regulatory subnetworks into nodule development. This notion is in line with the common principle of morphological evolution as proposed by Carroll,[59] in which changes in the spatial and temporal gene expression of preexisting developmental regulators and their associated downstream networks lead to trait divergence and the diversification of novel organ forms and functions. The parallel recruitment of a root initiation program and primordium identity program from the shoot that dictate nodule form and function are essential in non-legume species that are targets for engineering N fixation.

STAR★METHODS

Detailed methods are provided in the online version of this paper and include the following:

- KEY RESOURCES TABLE
- RESOURCE AVAILABILITY
  - Lead contact
  - Materials availability
  - Data and code availability
- EXPERIMENTAL MODEL AND SUBJECT DETAILS
  - Plant material and growth conditions
  - Bacterial strains
- METHOD DETAILS
  - Construct production
  - Hormone and chemical treatments
  - Gene expression analysis
  - Chromatin Immunoprecipitation (ChIP)
  - Next generation sequencing for RNA and Chromatin-Immunoprecipitation
  - Assessment of shoot-related phenotypes
  - Assessment of lateral root phenotypes
  - Acetylene reduction assay
  - Histochemical assays and cellular stains
  - Tissue Sections
  - mRNA in situ hybridization
  - Transmission electron microscopy analysis
  - Phylogenetic analysis
- QUANTIFICATION AND STATISTICAL ANALYSIS
  - RNA-seq
  - Clustering and Gene Ontology enrichment analysis
  - ChIP-Seq
  - qRTPCR
  - Phenotyping

SUPPLEMENTAL INFORMATION

Supplemental information can be found online at https://doi.org/10.1016/j.cub.2024.01.018.

ACKNOWLEDGMENTS

We thank Raymond Wightman, Gareth Evans, Kim Findlay, and Elaine Barclay for support with microscopy; Anne Edwards for help with the acetylene reduction assay; and Mandana Miri and Colleen Drapek for critical comments on the manuscript. We thank Pascal Ratet for providing *noot1/noot2* mutant seeds. K.S. thanks her orthopedic surgeon Dr. Erik Teumann, Eva Schiessl, and the families of Ingrid and Franz Trimmel and of Bernadette Gerstl for their care and support. This work was supported by the Bill and Melinda Gates Foundation and the UK Foreign, Commonwealth and Development Office (OPP1172165) through the Enabling Nutrient Symbioses in Agriculture (ENSA) project and the Gatsby Foundation (GAT3395/GLH).

AUTHOR CONTRIBUTIONS

K.S. designed and performed the experiments and analyzed the data with assistance from M.O., N.S., N.A.M.-R., and A.G.; T.L. analyzed RNA-seq and ChIP-seq data; M.B. performed and T.O. supervised dual histone reporter experiments; P.C.B. performed the phylogenetic analysis; M.B.B. provided resources and performed the acetylene reduction assay; K.S.M. and J.W. provided *Medicago* mutants; K.S. and G.E.D.O. supervised the work and wrote the manuscript.

DECLARATION OF INTERESTS

Related to this work, we submitted a Patent Cooperation Treaty (PCT) Application (PCT/IB2023/055144) on May 18th, 2023 under the title "PROTEINS FOR REGULATION OF SYMBIOTIC NODULE ORGAN IDENTITY."

Received: August 16, 2023
Revised: September 29, 2023
Accepted: January 8, 2024
Published: January 31, 2024

REFERENCES

1. Singh, S., Katzer, K., Lambert, J., Cerri, M., and Parniske, M. (2014). CYCLOPS, a DNA-binding transcriptional activator, orchestrates symbiotic root nodule development. Cell Host Microbe *15*, 139–152.
2. Marsh, J.F., Rakocevic, A., Mitra, R.M., Brocard, L., Sun, J., Eschstruth, A., Long, S.R., Schultze, M., Ratet, P., and Oldroyd, G.E. (2007). Medicago truncatula NIN is essential for rhizobial-independent nodule organogenesis induced by autoactive calcium/calmodulin-dependent protein kinase. Plant Physiol. *144*, 324–335.
3. Schauser, L., Roussis, A., Stiller, J., and Stougaard, J. (1999). A plant regulator controlling development of symbiotic root nodules. Nature *402*, 191–195.
4. Yoro, E., Suzaki, T., Toyokura, K., Miyazawa, H., Fukaki, H., and Kawaguchi, M. (2014). A Positive Regulator of Nodule Organogenesis, NODULE INCEPTION, Acts as a Negative Regulator of Rhizobial Infection in Lotus japonicus. Plant Physiol. *165*, 747–758.
5. Vernié, T., Kim, J., Frances, L., Ding, Y., Sun, J., Guan, D., Niebel, A., Gifford, M.L., de Carvalho-Niebel, F., and Oldroyd, G.E. (2015). The NIN Transcription Factor Coordinates Diverse Nodulation Programs in Different Tissues of the Medicago truncatula Root. Plant Cell *27*, 3410–3424.
6. Liu, J., Rasing, M., Zeng, T., Klein, J., Kulikova, O., and Bisseling, T. (2021). NIN is essential for development of symbiosomes, suppression of defence and premature senescence in Medicago truncatula nodules. New Phytol. *230*, 290–303.
7. Liu, J., Rutten, L., Limpens, E., Molen, T.v.d., Velzen, R.v., Chen, R., Chen, Y., Geurts, R., Kohlen, W., Kulikova, O., and Bisseling, T. (2019). A Remote cis-Regulatory Region Is Required for NIN Expression in the Pericycle to Initiate Nodule Primordium Formation in Medicago truncatula. Plant Cell *31*, 68–83.
8. Gonzalez-Rizzo, S., Crespi, M., and Frugier, F. (2006). The Medicago truncatula CRE1 cytokinin receptor regulates lateral root development and early symbiotic interaction with Sinorhizobium meliloti. Plant Cell *18*, 2680–2693.
9. Schiessl, K., Lilley, J.L.S., Lee, T., Tamvakis, I., Kohlen, W., Bailey, P.C., Thomas, A., Luptak, J., Ramakrishnan, K., Carpenter, M.D., et al. (2019). NODULE INCEPTION Recruits the Lateral Root Developmental Program for Symbiotic Nodule Organogenesis in Medicago truncatula. Curr. Biol. *29*, 3657–3668.e5.
10. Soyano, T., Shimoda, Y., Kawaguchi, M., and Hayashi, M. (2019). A shared gene drives lateral root development and root nodule symbiosis pathways in Lotus. Science *366*, 1021–1023.
11. Herrbach, V., Remblière, C., Gough, C., and Bensmihen, S. (2014). Lateral root formation and patterning in Medicago truncatula. J. Plant Physiol. *171*, 301–310.
12. Xiao, T.T., Schilderink, S., Moling, S., Deinum, E.E., Kondorosi, E., Franssen, H., Kulikova, O., Niebel, A., and Bisseling, T. (2014). Fate map of Medicago truncatula root nodules. Development *141*, 3517–3528.
13. Dong, W., Zhu, Y., Chang, H., Wang, C., Yang, J., Shi, J., Gao, J., Yang, W., Lan, L., Wang, Y., et al. (2021). An SHR-SCR module specifies legume cortical cell fate to enable nodulation. Nature *589*, 586–590.
14. Couzigou, J.M., Zhukov, V., Mondy, S., Abu el Heba, G., Cosson, V., Ellis, T.H., Ambrose, M., Wen, J., Tadege, M., Tikhonovich, I., et al. (2012). NODULE ROOT and COCHLEATA maintain nodule development and are legume orthologs of Arabidopsis BLADE-ON-PETIOLE genes. Plant Cell *24*, 4498–4510.
15. Magne, K., Couzigou, J.-M., Schiessl, K., Liu, S., George, J., Zhukov, V., Sahl, L., Boyer, F., Iantcheva, A., Mysore, K.S., et al. (2018). MtNODULE ROOT1 and MtNODULE ROOT2 Are Essential for Indeterminate Nodule Identity. Plant Physiol. *178*, 295–316.
16. Khan, M., Xu, H., and Hepworth, S.R. (2014). BLADE-ON-PETIOLE genes: Setting boundaries in development and defense. Plant Sci. *215–216*, 157–171.
17. Laloum, T., Baudin, M., Frances, L., Lepage, A., Billault-Penneteau, B., Cerri, M.R., Ariel, F., Jardinaud, M.-F., Gamas, P., de Carvalho-Niebel, F., and Niebel, A. (2014). Two CCAAT-box-binding transcription factors redundantly regulate early steps of the legume-rhizobia endosymbiosis. Plant J. *79*, 757–768.
18. Combier, J.P., Frugier, F., de Billy, F., Boualem, A., El-Yahyaoui, F., Moreau, S., Vernié, T., Ott, T., Gamas, P., Crespi, M., and Niebel, A. (2006). MtHAP2-1 is a key transcriptional regulator of symbiotic nodule development regulated by microRNA169 in Medicago truncatula. Genes Dev. *20*, 3084–3088.
19. Hossain, M.S., Shrestha, A., Zhong, S., Miri, M., Austin, R.S., Sato, S., Ross, L., Huebert, T., Tromas, A., Torres-Jerez, I., et al. (2016). Lotus japonicus NF-YA1 Plays an Essential Role During Nodule Differentiation and Targets Members of the SHI/STY Gene Family. Mol. Plant Microbe Interact. *29*, 950–964.
20. Shrestha, A., Zhong, S., Therrien, J., Huebert, T., Sato, S., Mun, T., Andersen, S.U., Stougaard, J., Lepage, A., Niebel, A., et al. (2020). Lotus japonicus Nuclear Factor YA1, a nodule emergence stage-specific regulator of auxin signalling. New Phytol. *229*, 1535–1552.
21. Feng, J., Lee, T., Schiessl, K., and Oldroyd, G.E.D. (2021). Processing of NODULE INCEPTION controls the transition to nitrogen fixation in root nodules. Science *374*, 629–632.
22. Baudin, M., Laloum, T., Lepage, A., Rípodas, C., Ariel, F., Frances, L., Crespi, M., Gamas, P., Blanco, F.A., Zanetti, M.E., et al. (2015). A Phylogenetically Conserved Group of Nuclear Factor-Y Transcription Factors Interact to Control Nodulation in Legumes. Plant Physiol. *169*, 2761–2773.
23. Soyano, T., Kouchi, H., Hirota, A., and Hayashi, M. (2013). Nodule inception directly targets NF-Y subunit genes to regulate essential processes of root nodule development in Lotus japonicus. PLoS Genet. *9*, e1003352.
24. Iyer, L.M., and Aravind, L. (2012). ALOG domains: provenance of plant homeotic and developmental regulators from the DNA-binding domain of a novel class of DIRS1-type retroposons. Biol. Direct *7*, 39.
25. Naramoto, S., Hata, Y., and Kyozuka, J. (2020). The origin and evolution of the ALOG proteins, members of a plant-specific transcription factor family, in land plants. J. Plant Res. *133*, 323–329.
26. He, L., Lei, Y., Li, X., Peng, Q., Liu, W., Jiao, K., Su, S., Hu, Z., Shen, Z., and Luo, D. (2020). SYMMETRIC PETALS 1 Encodes an ALOG Domain Protein that Controls Floral Organ Internal Asymmetry in Pea (Pisum sativum L.). Int. J. Mol. Sci. *21*, 4060.
27. Ye, Q., Zhu, F., Sun, F., Wang, T.-C., Wu, J., Liu, P., Shen, C., Dong, J., and Wang, T. (2022). Differentiation trajectories and biofunctions of symbiotic

and un-symbiotic fate cells in root nodules of Medicago truncatula. Mol. Plant *15*, 1852–1867.

28. Cho, E., and Zambryski, P.C. (2011). Organ boundary1 defines a gene expressed at the junction between the shoot apical meristem and lateral organs. Proc. Natl. Acad. Sci. USA *108*, 2154–2159.
29. MacAlister, C.A., Park, S.J., Jiang, K., Marcel, F., Bendahmane, A., Izkovich, Y., Eshed, Y., and Lippman, Z.B. (2012). Synchronization of the flowering transition by the tomato TERMINATING FLOWER gene. Nat. Genet. *44*, 1393–1398.
30. Yoshida, A., Sasao, M., Yasuno, N., Takagi, K., Daimon, Y., Chen, R., Yamazaki, R., Tokunaga, H., Kitaguchi, Y., Sato, Y., et al. (2013). TAWAWA1, a regulator of rice inflorescence architecture, functions through the suppression of meristem phase transition. Proc. Natl. Acad. Sci. USA *110*, 767–772.
31. Starker, C.G., Parra-Colmenares, A.L., Smith, L., Mitra, R.M., and Long, S.R. (2006). Nitrogen Fixation Mutants of Medicago truncatula Fail to Support Plant and Bacterial Symbiotic Gene Expression. Plant Physiol. *140*, 671–680.
32. Batzenschlager, M., Lace, B., Zhang, N., Su, C., Egli, S., Krohn, P., Salfeld, J., Ditengou, F.A., Laux, T., and Ott, T. (2023). Competence for transcellular infection in the root cortex involves a post-replicative, cell-cycle exit decision in Medicago truncatula. https://doi.org/10.1101/2023.03.28.534635.
33. Pecrix, Y., Staton, S.E., Sallet, E., Lelandais-Brière, C., Moreau, S., Carrère, S., Blein, T., Jardinaud, M.-F., Latrasse, D., Zouine, M., et al. (2018). Whole-genome landscape of Medicago truncatula symbiotic genes. Nat. Plants *4*, 1017–1025.
34. Mortier, V., Wasson, A., Jaworek, P., De Keyser, A., Decroos, M., Holsters, M., Tarkowski, P., Mathesius, U., and Goormachtig, S. (2014). Role of LONELY GUY genes in indeterminate nodulation on Medicago truncatula. New Phytol. *202*, 582–593.
35. Triozzi, P.M., Irving, T.B., Schmidt, H.W., Keyser, Z.P., Chakraborty, S., Balmant, K., Pereira, W.J., Dervinis, C., Mysore, K.S., Wen, J., et al. (2022). Spatiotemporal cytokinin response imaging and ISOPENTENYL TRANSFERASE 3 function in Medicago nodule development. Plant Physiol. *188*, 560–575.
36. Jarzyniak, K., Banasiak, J., Jamruszka, T., Pawela, A., Di Donato, M., Novák, O., Geisler, M., and Jasiński, M. (2021). Early stages of legume-rhizobia symbiosis are controlled by ABCG-mediated transport of active cytokinins. Nat. Plants *7*, 428–436.
37. Jamruszka, T., Banasiak, J., Pawela, A., Jarzyniak, K., Xia, J., Biała-Leonhard, W., Plačková, L., Iacobini, F.R., Novák, O., Geisler, M., and Jasiński, M. (2022). Medicago truncatula ABCG40 is a cytokinin importer negatively regulating lateral root density and nodule number. https://doi.org/10.1101/2022.11.10.516000.
38. Lohar, D.P., Schaff, J.E., Laskey, J.G., Kieber, J.J., Bilyeu, K.D., and Bird, D.M. (2004). Cytokinins play opposite roles in lateral root formation, and nematode and Rhizobial symbioses. Plant J. *38*, 203–214.
39. Tan, S., Sanchez, M., Laffont, C., Boivin, S., Le Signor, C., Thompson, R., Frugier, F., and Brault, M. (2020). A Cytokinin Signaling Type-B Response Regulator Transcription Factor Acting in Early Nodulation. Plant Physiol. *183*, 1319–1330.
40. Vinardell, J.M., Fedorova, E., Cebolla, A., Kevei, Z., Horvath, G., Kelemen, Z., Tarayre, S., Roudier, F., Mergaert, P., Kondorosi, A., and Kondorosi, E. (2003). Endoreduplication Mediated by the Anaphase-Promoting Complex Activator CCS52A Is Required for Symbiotic Cell Differentiation in Medicago truncatula Nodules. Plant Cell *15*, 2093–2105.
41. Franssen, H.J., Xiao, T.T., Kulikova, O., Wan, X., Bisseling, T., Scheres, B., and Heidstra, R. (2015). Root developmental programs shape the Medicago truncatula nodule meristem. Development *142*, 2941–2950.
42. Santuari, L., Sanchez-Perez, G.F., Luijten, M., Rutjens, B., Terpstra, I., Berke, L., Gorte, M., Prasad, K., Bao, D., Timmermans-Hereijgers, J.L., et al. (2016). The PLETHORA Gene Regulatory Network Guides Growth and Cell Differentiation in Arabidopsis Roots. Plant Cell *28*, 2937–2951.
43. Galinha, C., Hofhuis, H., Luijten, M., Willemsen, V., Blilou, I., Heidstra, R., and Scheres, B. (2007). PLETHORA proteins as dose-dependent master regulators of Arabidopsis root development. Nature *449*, 1053–1057.
44. Carrere, S., Verdier, J., and Gamas, P. (2021). MtExpress, a Comprehensive and Curated RNAseq-based Gene Expression Atlas for the Model Legume Medicago truncatula. Plant Cell Physiol. *62*, 1494–1500.
45. Xu, C., Park, S.J., Van Eck, J., and Lippman, Z.B. (2016). Control of inflorescence architecture in tomato by BTB/POZ transcriptional regulators. Genes Dev. *30*, 2048–2061.
46. Laporte, P., Lepage, A., Fournier, J., Catrice, O., Moreau, S., Jardinaud, M.-F., Mun, J.-H., Larrainzar, E., Cook, D.R., Gamas, P., and Niebel, A. (2014). The CCAAT box-binding transcription factor NF-YA1 controls rhizobial infection. J. Exp. Bot. *65*, 481–494.
47. Gauthier-Coles, C., White, R.G., and Mathesius, U. (2018). Nodulating Legumes Are Distinguished by a Sensitivity to Cytokinin in the Root Cortex Leading to Pseudonodule Development. Front. Plant Sci. *9*, 1901.
48. Dello Ioio, R.D., Nakamura, K., Moubayidin, L., Perilli, S., Taniguchi, M., Morita, M.T., Aoyama, T., Costantino, P., and Sabatini, S. (2008). A Genetic Framework for the Control of Cell Division and Differentiation in the Root Meristem. Science *322*, 1380–1384.
49. Laplaze, L., Benkova, E., Casimiro, I., Maes, L., Vanneste, S., Swarup, R., Weijers, D., Calvo, V., Parizot, B., Herrera-Rodriguez, M.B., et al. (2007). Cytokinins Act Directly on Lateral Root Founder Cells to Inhibit Root Initiation. Plant Cell *19*, 3889–3900.
50. Marhavý, P., Bielach, A., Abas, L., Abuzeineh, A., Duclercq, J., Tanaka, H., Pařezová, M., Petrášek, J., Friml, J., Kleine-Vehn, J., and Benková, E. (2011). Cytokinin Modulates Endocytic Trafficking of PIN1 Auxin Efflux Carrier to Control Plant Organogenesis. Dev. Cell *21*, 796–804.
51. Marhavý, P., Duclercq, J., Weller, B., Feraru, E., Bielach, A., Offringa, R., Friml, J., Schwechheimer, C., Murphy, A., and Benková, E. (2014). Cytokinin Controls Polarity of PIN1-Dependent Auxin Transport during Lateral Root Organogenesis. Curr. Biol. *24*, 1031–1037.
52. Dello Ioio, R., Linhares, F.S., Scacchi, E., Casamitjana-Martinez, E., Heidstra, R., Costantino, P., and Sabatini, S. (2007). Cytokinins Determine Arabidopsis Root-Meristem Size by Controlling Cell Differentiation. Curr. Biol. *17*, 678–682.
53. Reid, D.E., Heckmann, A.B., Novák, O., Kelly, S., and Stougaard, J. (2016). CYTOKININ OXIDASE/DEHYDROGENASE3 Maintains Cytokinin Homeostasis during Root and Nodule Development in Lotus japonicus. Plant Physiol. *170*, 1060–1074.
54. Gamas, P., Brault, M., Jardinaud, M.F., and Frugier, F. (2017). Cytokinins in Symbiotic Nodulation: When, Where, What For? Trends Plant Sci. *22*, 792–802.
55. Cooper, J.B., and Long, S.R. (1994). Morphogenetic Rescue of Rhizobium meliloti Nodulation Mutants by trans-Zeatin Secretion. Plant Cell *6*, 215–225.
56. Soyano, T., Hirakawa, H., Sato, S., Hayashi, M., and Kawaguchi, M. (2014). Nodule Inception creates a long-distance negative feedback loop involved in homeostatic regulation of nodule organ production. Proc. Natl. Acad. Sci. USA *111*, 14607–14612.
57. Fan, W., Xia, C., Wang, S., Liu, J., Deng, L., Sun, S., and Wang, X. (2022). Rhizobial infection of 4C cells triggers their endoreduplication during symbiotic nodule development in soybean. New Phytol. *234*, 1018–1030.
58. Griesmann, M., Chang, Y., Liu, X., Song, Y., Haberer, G., Crook, M.B., Billault-Penneteau, B., Lauressergues, D., Keller, J., Imanishi, L., et al. (2018). Phylogenomics reveals multiple losses of nitrogen-fixing root nodule symbiosis. Science *361*, eaat1743.
59. Carroll, S.B. (2008). Evo-Devo and an Expanding Evolutionary Synthesis: A Genetic Theory of Morphological Evolution. Cell *134*, 25–36.
60. Lerouge, P., Roche, P., Faucher, C., Maillet, F., Truchet, G., Promé, J.C., and Dénarié, J. (1990). Symbiotic host-specificity of Rhizobium meliloti is determined by a sulphated and acylated glucosamine oligosaccharide signal. Nature *344*, 781–784.

61. Boisson-Dernier, A., Chabaud, M., Garcia, F., Bécard, G., Rosenberg, C., and Barker, D.G. (2001). Agrobacterium rhizogenes-Transformed Roots of Medicago truncatula for the Study of Nitrogen-Fixing and Endomycorrhizal Symbiotic Associations. Mol. Plant Microbe Interact. *14*, 695–700.

62. Ehrhardt, D.W., Atkinson, E.M., and Long, S.R. (1992). Depolarization of alfalfa root hair membrane potential by Rhizobium meliloti Nod factors. Science *256*, 998–1000.

63. Ursache, R., Andersen, T.G., Marhavý, P., and Geldner, N. (2018). A protocol for combining fluorescent proteins with histological stains for diverse cell wall components. Plant J. *93*, 399–412.

64. Cheng, X., Wang, M., Lee, H.-K., Tadege, M., Ratet, P., Udvardi, M., Mysore, K.S., and Wen, J. (2014). An efficient reverse genetics platform in the model legume Medicago truncatula. New Phytol. *201*, 1065–1076.

65. Plet, J., Wasson, A., Ariel, F., Le Signor, C., Baker, D., Mathesius, U., Crespi, M., and Frugier, F. (2011). MtCRE1-dependent cytokinin signaling integrates bacterial and plant cues to coordinate symbiotic nodule organogenesis in Medicago truncatula. Plant J. *65*, 622–633.

66. Weber, E., Engler, C., Gruetzner, R., Werner, S., and Marillonnet, S. (2011). A Modular Cloning System for Standardized Assembly of Multigene Constructs. PLoS One *6*, e16765.

67. Rokhsar, D.S., Fazo, J., Putnam, N., Hayes, R.D., Neupane, R., Howson, R., Shu, S., Mitros, T., Hellsten, U., Dirks, W., and Goodstein, D.M. (2011). Phytozome: a comparative platform for green plant genomics. Nucleic Acids Res. *40*, D1178–D1186.

68. Tang, H., Krishnakumar, V., Bidwell, S., Rosen, B., Chan, A., Zhou, S., Gentzbittel, L., Childs, K.L., Yandell, M., Gundlach, H., et al. (2014). An improved genome release (Version Mt4.0) for the model legume Medicago truncatula. BMC Genomics *15*, 312.

69. Dobin, A., Davis, C.A., Schlesinger, F., Drenkow, J., Zaleski, C., Jha, S., Batut, P., Chaisson, M., and Gingeras, T.R. (2013). STAR: ultrafast universal RNA-seq aligner. Bioinformatics *29*, 15–21.

70. Liao, Y., Smyth, G.K., and Shi, W. (2014). featureCounts: an efficient general purpose program for assigning sequence reads to genomic features. Bioinformatics *30*, 923–930.

71. Love, M.I., Huber, W., and Anders, S. (2014). Moderated estimation of fold change and dispersion for RNA-seq data with DESeq2. Genome Biol. *15*, 550.

72. Andrews, S. (2010). FastQC: a quality control tool for high throughput sequence data. http://www.bioinformatics.babraham.ac.uk/projects/fastqc.

73. Leek, J.T., Johnson, W.E., Parker, H.S., Jaffe, A.E., and Storey, J.D. (2012). The sva package for removing batch effects and other unwanted variation in high-throughput experiments. Bioinformatics *28*, 882–883.

74. Mächler, M., Rousseeuw, P., Struyf, A., Hubert, M., and Hornik, K. (2012). Cluster: Cluster Analysis Basics and Extensions. https://CRAN.R-project.org/package=cluster.

75. Alexa, A., and Rahnenführer, J. (2009). Gene set enrichment analysis with topGO. Bioconductor Improv. *27*, 1–26.

76. Gu, Z., Eils, R., and Schlesner, M. (2016). Complex heatmaps reveal patterns and correlations in multidimensional genomic data. Bioinformatics *32*, 2847–2849.

77. Landt, S.G., Marinov, G.K., Kundaje, A., Kheradpour, P., Pauli, F., Batzoglou, S., Bernstein, B.E., Bickel, P., Brown, J.B., Cayting, P., et al. (2012). ChIP-seq guidelines and practices of the ENCODE and modENCODE consortia. Genome Res. *22*, 1813–1831.

78. Langmead, B., and Salzberg, S.L. (2012). Fast gapped-read alignment with Bowtie 2. Nat. Methods *9*, 357–359.

79. Zhang, Y., Liu, T., Meyer, C.A., Eeckhoute, J., Johnson, D.S., Bernstein, B.E., Nusbaum, C., Myers, R.M., Brown, M., Li, W., and Liu, X.S. (2008). Model-based Analysis of ChIP-Seq (MACS). Genome Biol. *9*, R137.

80. Yu, G., Wang, L.G., and He, Q.Y. (2015). ChIPseeker: an R/Bioconductor package for ChIP peak annotation, comparison and visualization. Bioinformatics *31*, 2382–2383.

81. Quinlan, A.R., and Hall, I.M. (2010). BEDTools: a flexible suite of utilities for comparing genomic features. Bioinformatics *26*, 841–842.

82. Ramírez, F., Ryan, D.P., Grüning, B., Bhardwaj, V., Kilpert, F., Richter, A.S., Heyne, S., Dündar, F., and Manke, T. (2016). deepTools2: a next generation web server for deep-sequencing data analysis. Nucleic Acids Res. *44*, W160–W165.

83. Schindelin, J., Arganda-Carreras, I., Frise, E., Kaynig, V., Longair, M., Pietzsch, T., Preibisch, S., Rueden, C., Saalfeld, S., Schmid, B., et al. (2012). Fiji: an open-source platform for biological-image analysis. Nat. Methods *9*, 676–682.

84. Stamatakis, A. (2014). RAxML version 8: a tool for phylogenetic analysis and post-analysis of large phylogenies. Bioinformatics *30*, 1312–1313.

85. Letunic, I., and Bork, P. (2016). Interactive tree of life (iTOL) v3: an online tool for the display and annotation of phylogenetic and other trees. Nucleic Acids Res. *44*, W242–W245.

86. Cortijo, S., Charoensawan, V., Roudier, F., and Wigge, P.A. (2018). Chromatin Immunoprecipitation Sequencing (ChIP-Seq) for Transcription Factors and Chromatin Factors in Arabidopsis thaliana Roots: From Material Collection to Data Analysis. Methods Mol. Biol. *1761*, 231–248.

87. Schiessl, K., Muiño, J.M., and Sablowski, R. (2014). Arabidopsis JAGGED links floral organ patterning to tissue growth by repressing Kip-related cell cycle inhibitors. Proc. Natl. Acad. Sci. USA *111*, 2830–2835.

88. Dilworth, M.J. (1966). Acetylene reduction by nitrogen-fixing preparations from Clostridium pasteurianum. Biochim. Biophys. Acta *127*, 285–294.

89. Schöllhorn, R., and Burris, R.H. (1967). Acetylene as a competitive inhibitor of N-2 fixation. Proc. Natl. Acad. Sci. USA *58*, 213–216.

90. Zhang, W., and Wen, C.K. (2010). Preparation of ethylene gas and comparison of ethylene responses induced by ethylene, ACC, and ethephon. Plant Physiol. Biochem. *48*, 45–53.

91. Yang, W., Cortijo, S., Korsbo, N., Roszak, P., Schiessl, K., Gurzadyan, A., Wightman, R., Jönsson, H., and Meyerowitz, E. (2021). Molecular mechanism of cytokinin-activated cell division in Arabidopsis. Science *371*, 1350–1355.

92. Tibshirani, R., Walther, G., and Hastie, T. (2001). Estimating the Number of Clusters in a Data Set via the Gap Statistic. J. R. Stat. Soc. B *63*, 411–423.

93. Ward, J.H. (1963). Hierarchical Grouping to Optimize an Objective Function. J. Am. Stat. Assoc. *58*, 236–244.

94. Harris, M.A., Clark, J., Ireland, A., Lomax, J., Ashburner, M., Foulger, R., Eilbeck, K., Lewis, S., Marshall, B., Mungall, C., et al. (2004). The Gene Ontology (GO) database and informatics resource. Nucleic Acids Res. *32*, D258–D261.

95. Pfaffl, M.W. (2001). A new mathematical model for relative quantification in real-time RT-PCR. Nucleic Acids Res. *29*, e45.

STAR★METHODS

KEY RESOURCES TABLE

REAGENT or RESOURCE	SOURCE	IDENTIFIER
Antibodies		
µMACS Anti-GFP Starting Kit	Miltenyi Biotec	130-091-288; RRID: AB_247003
Bacterial and Virus Strains		
Sinorhizobium meliloti strain 2011	Lerouge et al.[60]	N/A
Sinorhizobium meliloti strain 2011 *pXLGD4 lacZ strain*	Lerouge et al.[60]	N/A
Agrobacterium rhizogenes strain AR1193	Boisson-Dernier et al.[61]	N/A
Sinorhizobium meliloti strain 2011 *mCherry*	Starker et al.[31]	N/A
Chemicals, Peptides, and Recombinant Proteins		
buffered nodulation media (BMN)	Ehrhardt et al.[62]	N/A
Fahraeus media (FP)	Boisson-Dernier et al.[61]	N/A
cOmplete, Mini, EDTA-freier Protease-Inhibitor-Cocktail	Roche	11836170001
PCR purification Kit	Qiagen	28104
DIG RNA Labeling Kit	Roche	11175025910
NBT	Roche	11383213001
Anti-digoxigenin-AP-Fab	Roche	11093274910
BCIP	Roche	11383221001
Dextran sulfate salt	Sigma	D8906-5G
Denhards powder	Sigma	D2532 5ml
ClearSee	Ursache et al.[63]	N/A
Luteolin	Sigma-Aldrich	L9283,CAS: 491-70-3
RNeasy Micro Kit	Qiagen	Cat 74004
RNase free DNase Kit	Qiagen	Cat 79254
5-Bromo-4-chloro-3-indolyl-β-D-glucuronic acid, sodium salt trihydrate	Melford Laboratories	CAS:12954-41-9
5-Bromo-4-chloro-3-indolyl β-D-galactopyranoside (x-gal)	Sigma-Aldrich	B4252, CAS: 7240-90-6
Magenta-5-Bromo-6-chloro-3-indolyl-β-D-galactopyranoside (magenta-x-gal)	Melford Laboratories	CAS: 93863-88-8
Propidium iodide	Sigma-Aldrich	P4170, CAS:25535-16-4
Fluorescent Brightener 28 disodium salt solution	Sigma-Aldrich	910090, CAS: 4193-55-9
5-ethynyl-2'-deoxyuridine (EdU)	Invitrogen	A10044
Alexa Fluor™ 488 5-Carboxamido-(6-Azidohexanyl), Bis(Triethylammonium Salt)), 5-isomer	Invitrogen	A10266
α-Amylase from Bacillus licheniformis	Sigma-Aldrich	A3403, CAS: 9000-85-5
RNA Transcriptor First Strand cDNA Synthesis Kit	Roche Diagnostics	04379012001
LightCycler 480 SYBR green I master	Roche Diagnostics	04707516001
6-Benzylaminopurine	Sigma-Aldrich	B3408, CAS:1214-39-7
Technovit 7100	Kulzer Technik	64709003
Ruthenium Red	Sigma-Aldrich	R2751, CAS: 11103-72-3
Ethephon	Sigma-Aldrich	C0143, CAS: 16672-87-0
BD Vacutainer Tubes	Thermo Fisher Scientific	362725
Chloral hydrate	Sigma-Aldrich	C8383, CAS:302-17-0
Critical Commercial Assays		
Illumina TruSeq Stranded mRNA HT kit & sequencing	Illumina, sequencing performed by Novogene Europe	RS-122-2001
Illumina TruSeq® Stranded mRNA HT kit and ChIP-Seq library kit & sequencing	Illumina, sequencing performed by Novogene Europe	IP-202-1012

(*Continued on next page*)

Continued

REAGENT or RESOURCE	SOURCE	IDENTIFIER
Deposited Data		
Short read sequencing data (RNA-Seq and Chip-Seq data)	this manuscript	Gene expression Omnibus GSE211680 and GSE243570
Experimental Models: Organisms/Strains		
Medicago truncatula cultivar jemalong	Heritage Seeds Pty. Ltd., Adelaide, AU	jemalong
Medicago truncatula ecotype R108 incl tnt insertion lines *NF17203 (lsh1-1), NF1304 (lsh1-2), NF14992 (lsh2-1)* originally obtained from Nobel Research institute LLC, Ardmore, USA; Cheng et al.[64]	this manuscript	*lsh1-1, lsh1-2, lsh2-1*
Medicago truncatula ecotype A17 mutant *cre1-1*	Plet et al.[65]	*cre1-1*
Medicago truncatula ecotype A17 mutant *nin-1*	Marsh et al.[2]	*nin-1*
Medicago truncatula ecotype A17 mutant *nfya1-1*	Laporte et al.[46]	*nfya1-1*
Medicago truncatula ecotype R108 mutant *noot1-1/ noot2-1*	Magne et al.[15]	*noot1-1/noot2-1*
Oligonucleotides		
For qRTPCR and genotyping oligos see Table S5	this manuscript	N/A
Recombinant DNA		
Golden Gate Level 0, distributed via https://www.ensa.ac.uk	GeneArt, Thermo Fisher Scientific	N/A
Binary plasmids generated using Golden Gate Cloning; Weber et al.,[66] details see Table S6	this manuscript	N/A
Software and Algorithms		
Sequence info *M. truncatula* Mt4.0v1 genome retrieved Phytozome https://phtyozome.jgi.doe.gov	Rokhsar et al.[67]; Tang et al.[68]	N/A
M. truncatula reference genome version v5.1.9	Pecrix et al.[33]	N/A
STAR (v2.7.10b)	Dobin et al.[69]	N/A
featureCounts in R package Rsubread (v2.12.0)	Liao et al.[70]	N/A
R package DESeq2	Love et al.[71]	N/A
fastQC software	Andrews[72]	N/A
R sva (v3.46.0)	Leek et al.[73]	N/A
R package cluster (v2.1.4)	Mächler et al.[74]	N/A
topGO (v2.50.0)	Alexa and Rahnenführer[75]	N/A
R package ComplexHeatmap (2.14.0)	Gu et al.[76]	N/A
ENCOD-DCC ChIP-Seq pipeline2 version 2.1.2	Landt et al.[77]	N/A
Bowtie 2 tool	Langmead and Salzberg[78]	N/A
macs2	Zhang et al.[79]	N/A
ChIPseeker R package	Yu et al.[80]	N/A
BEDToolsbedtools	Quinlan and Hall[81]	N/A
deepTools2 bamCompare	Ramirez et al.[82]	N/A
Synonym locus ID matches obtained from Uniprot	Uniprot, 2018	N/A
Confocal imaging analysis software FIJI	Schindelin et al.[83]	N/A
HMMER3.1b2 HMMSEARCH, HMMALIGN	https://hmmer.org	N/A
MPI version of RAxML v8.2.9	Stamatakis[84]	N/A
Interactive Tree of Life Visualisation Tool iToL	Letunic and Bork[85]	N/A
Lotus genome annotation retrieved	ftp://ftp.kazusa.or.jp/pub/lotus/	N/A
Arabidopsis (Araport11) genome annotation retrieved	www.arabidopsis.org	N/A
Solanum & Medicago genome annotation retrieved	Phytozome, V10	N/A
Pisum genome annotation retrieved	https://urgi.versailles.inra.fr/Species/Pisum, v1a	N/A
Original code compiled for this manuscript	this manuscript	https://github.com/LeeeTak/Lee_Currentbiology

RESOURCE AVAILABILITY

Lead contact

Further information and requests for resources and reagents should be directed to and will be fulfilled by the lead contact Katharina Schiessl (ks846@cam.ac.uk) subject to material transfer agreements.

Materials availability

Plasmids and plant loss of function muntant lines generated in this study are available from the lead contact upon request.

Data and code availability

- The short-read sequencing data (ChIP-Seq and RNA-Seq data) generated in this study have been deposited at the National Center for Biotechnology Information Gene Expression Omnibus, with accession numbers GSE211680 and GSE243570 and are publicly available as of the date of publication. Lists of differentially expressed genes and ChIP-Seq targets and downstream analyses are compiled in Data S1 and S2. Accession numbers are listed in the key resources table in the "Deposited Data" section.
- All original code has been deposited at GitHub https://github.com/LeeeTak/Lee_Currentbiology and is publicly available as of the date of publication. Original code is listed in the key resources table in the ‘‘Software and Algorithms’’ section.
- Any additional information required to reanalyze the data reported in this paper is available from the lead contact upon request.

EXPERIMENTAL MODEL AND SUBJECT DETAILS

Plant material and growth conditions

M. truncatula ecotypes *jemalong*, cultivar Jester, and ecotype *R108* were used as wildtype in this study, dependent on the ecotype of the respective mutant. *Jemalong* was used to perform hairy root transformations and as wildtype for comparisons to *cre-1*, *nin-1*, and *nfy-a1-1*, previously described.[2,65] All Tnt1 retrotransposon insertion lines described in this manuscript (*NF17203 (lsh1-1)*, *NF1304 (lsh1-2)* and *NF14992* (*lsh2-1*) were derivatives of the R108 ecotype and obtained from the Tnt1 Retrotransposon Mutant Collection (Oklahoma State University, Stillwater, USA; previously Noble Research Institute, LLC., Ardmore USA).[64] Previously described *NF2717* (*noot1-1*), *NF5464* (*noot2-1*) were used.[15] R108 was used as the wildtype for analysis of these Tnt1 mutants. Genotyping was performed using Tnt1-F and Tnt1-R oligos combined with the corresponding forward and reverse oligos encompassing the insertions (Table S5).

Seeds were scarified, surface sterilized with 10% (v/v) bleach solution, stratified for 3 days at 4 °C and germinated on water agar plates. Plants were grown in sterile conditions in controlled environment rooms at 22 °C (80% humidity, 16 h light/8 h dark, 300 μmol m2 s-1 light intensity) on filter paper-lined agar media in sealed plates unless otherwise specified. For Chromatin-Immunoprecipitation and assessment of the root phenotype in the over-expression lines, hairy roots were grown on modified Fahraeus medium supplemented with 0.5 mM NH4NO3[61] for 3 weeks.

For rhizobial spot inoculation seedlings were grown for 2 days on buffered nodulation medium (BNM)[62] supplemented with 1 μM aminoethoxyvinylglycine (AVG; Sigma-Aldrich Company Ltd, Darmstadt, Germany) at 22 °C (16 hours light/8 hours dark, 300 μmol m-2 s-1 light intensity). *Sinorhizobium meliloti* strain 2011[60] was grown in minimal medium supplemented with 3 μM luteolin (Sigma-Aldrich Company Ltd, Darmstadt, Germany) and diluted to a final concentration of 0.02 OD 600 nm using Fahraeus medium.[61] The mock treatment consisted of Fahraeus medium with luteolin diluted to an equivalent concentration as the inoculum. Approximately 1 μL of *S. meliloti* suspension or mock treatment was inoculated onto the susceptibility zone (where the root hairs first appear) and marked by puncturing the filter paper alongside the site of inoculation. After 24 and 72 hours, 2 mm sections of the root alongside the site of inoculation were harvested for RNA isolation or microscopy.

For spray inoculation of *S. meliloti* for plants grown on plates, seedlings were grown under similar conditions as described above. Roots of 1-day-old seedlings were covered with filter paper and sprayed with 2 ml *S. meliloti* of final concentration 0.02 OD 600 nm grown in minimal medium without luteolin. For inoculation of hairy roots and for phenotyping assays of mature nodules, plants were transferred to terragreen:sharp sand mix (1:1) (Oil-DriCompany, Wisbech, UK) in P40 trays and left to grow for 7 days before inoculation with *S. meliloti 2011* (2 mL of overnight culture per plant diluted in liquid BNM to 0.02 OD 600 nm). Plants were grown for up to a further 4 weeks for nodule quantification and histochemical staining.

Bacterial strains

Sinorhizobium meliloti 2011 expressing *pXLGD4 (hemA: lacZ), pNifH:GUS*, or *mCherry* were used in this study.[31,60] *Agrobacterium rhizogenes* strain AR1193 was used to introduce all binary vectors used in this study (*DsRed* as transformation marker) to *M. truncatula jemalong* seedlings following a previously published transient hairy root transformation protocol.[61]

METHOD DETAILS

Construct production

The Golden Gate modular cloning system was used to prepare the plasmids.[66] All Level 0s used in this study are held for distribution in the ENSA project core collection (https://www.ensa.ac.uk/) and are listed along with the binary plasmid details in Table S1A. Sequences were domesticated, synthesized and cloned into pMS (GeneArt, Thermo Fisher Scientific, Waltham, USA). Sequence information for *LSH1* (*Medtr1g069825*), *LSH2 (Medtr7g097030), NF-YA1 (Medtr1g056530), NOOT1 (Medtr7g090020)* and *NOOT2 (Medtr1g051025)* were obtained from the *M. truncatula* Mt4.0v1 genome via Phytozome (https://phytozome.jgi.doe.gov).[67,68]

Hormone and chemical treatments

6-Benzylaminopurine (BAP; Sigma-Aldrich Company Ltd, Darmstadt, Germany) were dissolved in water. Mock treatments were equal volumes of each solvent in the agar media. For BAP plate treatments (100 nM), 2-day old seedlings were grown on BNM plates for 24 hours with either BAP or mock and supplemented with 1 μM AVG to replicate spot inoculation conditions.

Gene expression analysis

For rhizobial spot inoculation time-course experiments, roots were dissected as 2- to 3-mm segments around the spot of inoculation or mock treatment. For BAP response experiments, segments were dissected around the susceptibility zone marked at the time of treatment. About 50 to 60 segments were pooled to obtain 1 biological replicate, with 3-6 biological replicates per treatment/genotype were analyzed. RNA was extracted using the RNeasy Micro Kit (Qiagen, Germantown, USA) and the RNase free DNase kit (Qiagen, Germantown, USA) was used to remove genomic DNA. For reverse transcription of 1 μg total RNA, Transcriptor First Strand cDNA Synthesis Kit was used according to the manufacturer's instructions (Roche Diagnostics GmbH). Quantitative real-time polymerase chain reactions (qRT-PCR) were performed in technical triplicates in the LightCycler 480 System using LightCycler 480 SYBR green I master (04707516001, Roche Diagnostics GmbH, Mannheim, Germany) in a total reaction volume of 10 μl. The primer pairs used for gene expression analysis are listed in Table S1A.

Chromatin Immunoprecipitation (ChIP)

ChIP was performed using a combination of two protocols.[86,87] Transiently transformed 3-week old *M. truncatula* hairy roots in the ecotype *jemalong* expressing *pLjUBI:GFP-LSH1*, *pLjUBI:GFP-NIN* or control *pLjUBI:NLS-GPF* grown under non-symbiotic conditions were used. Root tissue [2000–3000 mg (fresh weight) per sample] were fixed in 35 mL of fixation buffer [NaHPO4 (100 mM) buffer, 1% formaldehyde, 100 μM PMSF] under vacuum for 20 min on ice. Cross-linking was stopped with 100 μM glycine for 10 min on ice. Tissue was washed twice with water, frozen in liquid nitrogen and stored at -80°C. Ground tissue was resuspended in 25 ml extraction buffer 1 (10 mM Tris-HCl pH 8, 10 mM MgCl2, 0.4 M sucrose, 100 μM PMSF, 10 mM ß-mercaptoethanol, 1 tablet (per 50 ml of buffer) of protease inhibitor cocktail complete Mini, EDTA-free (11836170001, Roche)), filtered through miracloth and centrifuged at 1800 x g for 20 min at 4°C. The pellet was resuspended in 10 ml extraction buffer 2 (10 mM Tris-HCl pH 8, 10 mM $MgCl_2$, 0.24 M sucrose, 100 μM PMSF, 10 mM ß-mercaptoethanol, 1% Triton, 1 tablet (per 50 ml of buffer) of protease inhibitor cocktail complete Mini, EDTA-free (11836170001, Roche)) and centrifuged at 1800 x g for 10 min at 4°C. This washing step was repeated twice, followed by three washes with extraction buffer 3 (10 mM Tris-HCl pH 8, 10 mM $MgCl_2$, 1.70 M sucrose, 100 μM PMSF, 10 mM ß-mercaptoethanol, 0.15% Triton, 1 tablet (per 50 ml of buffer) of protease inhibitor cocktail complete Mini, EDTA-free (11836170001, Roche)) as described in Cortijo et al.[86] Purified nuclei pellets were resuspended in 1 mL of sonication buffer containing 500 mM Hepes, 150 mM NaCl, 5 mM MgCl2, 10% (vol/vol) TRITON X-100, and one-half of a tablet of protease inhibitor mixture complete Mini, EDTA-free (Roche). Sonication was performed in a Bioruptor water bath sonicator at 4 °C (3 × 6 min high-power level with 30 s on/30 s off cycles), resulting in an average fragment size of 300-500 bp. After centrifugation, the supernatant was mixed with 500 μL of immunoprecipitation buffer containing 0.5 M Hepes, 150 mM NaCl, 5 mM $MgCl_2$, 10% (vol/vol) TRITON X-100, 1 mg/mL BSA, and 25 μL of anti-GFP μMACS Microbeads (Miltenyi Biotec); incubated on ice for 30 min; and loaded on a μ Column (Miltenyi Biotec) that had been equilibrated with 200 μL of immunoprecipitation buffer and placed into a magnetic μMACS separator (Miltenyi Biotec). After washing four times with 200 - 400 μL of immunoprecipitation buffer and twice with 200 μL of TE buffer [100 mM Tris (pH 8), 10 mM EDTA (pH 8)], DNA was eluted once with 20 μL and twice with 50 μL of preheated (96 °C) elution buffer containing 50 mM Tris (pH 8), 10 mM EDTA, 50 mM DTT, and 1% SDS. One hundred microliters of TE buffer and 9 μL of 25 mg/mL Proteinase K (Sigma) were added to the eluted samples and to the input control samples. Cross-linking was reverted in eluted and input samples at 37 °C overnight, followed by addition of 9 μL of 25 mg/mL Proteinase K and 8 h of incubation at 65 °C, phenol-chloroform extraction, and precipitation with ethanol overnight at −20 °C. After washing in 70% (vol/vol) EtOH, the air-dried DNA was resuspended in 100 μL of PCR-grade water (Roche), purified using a PCR purification Kit (catalog no. 18104; Qiagen), and stored at −80 °C.

Next generation sequencing for RNA and Chromatin-Immunoprecipitation

RNA sequencing (RNA-Seq) and sequencing following Chromatin-Immunopreciptiation sequencing (ChIP-Seq) were performed by Novogene Europe (Cambridge, UK). RNA-Seq and ChIP-Seq libraries were prepared with the Illumina TruSeq® Stranded mRNA HT kit and ChIP-Seq library kit, respectively. The sequencing of the libraries was performed on the Illumina NovaSeq 6000 next generation sequencing system with the read length of 150 bp paired-end reads resulting in 20 million reads and 15-30 million reads per sample for RNA-Seq and ChIP-Seq, respectively.

Assessment of shoot-related phenotypes

Flowers and stipules were dissected from the main shoot, arranged on double-sided tape and directly imaged using the Keyence VHX-5000 microscope equipped with a range of zoom lenses from 20x to 1000x (Keyence Ltd, Milton Keynes, UK).

Assessment of lateral root phenotypes

Seedlings were grown on modified Fahraeus medium[61] plates for 14 days before lateral root number and length was scored.

Acetylene reduction assay

Nitrogenase activity was measured *in vivo* in mature nodules of terragreen:sand grown plants at 21 days post inoculation with *S. meliloti 2011* by the acetylene reduction assay.[88,89] Freshly harvested nodules were immediately transferred to BD Vacutainer tubes (3ml, 13x75mm, Thermo Fisher Scientific, Waltham, USA) prior to the injection of 10% (v/v) acetylene (C_2H_2). After 1 hour incubation, ethylene (C_2H_4) was quantified using a Perkin Elmer Clarus 480 gas chromatograph equipped with a HayeSep® N (80-100 MESH) column. The injector and oven temperatures were kept at 100 °C, while the FID detector was set at 150 °C. The carrier gas (nitrogen) flow was set at 8 - 10 mL/min. An ethylene calibration curve was prepared from chemical decomposition of ethephon (Sigma C0143) in 10 mM Na2HPO4 pH 10.7 as described previously.[90] Nitrogenase activity is reported as nmol of C_2H_4 per nodule per min.

Histochemical assays and cellular stains

For GUS staining roots were washed in water and immediately fixed in 90% acetone on ice for 1 hr. Subsequently, the acetone was replaced by a wash solution containing 50 mM phosphate buffer pH 7.2. The wash buffer was replaced by GUS staining buffer containing 50 mM phosphate buffer pH 7.2, 0.5 mM K3Fe(CN)6 (potassium ferricyanide), 0.5 mM K4Fe(CN)6 (potassium ferrocyanide) and 2 mM 5-bromo-4-chloro-3-indolyl-beta-D-glucuronide (X-Gluc, Melford Laboratories Ltd., Ipswich, UK), vacuum infiltrated for 15 min and incubated at 37°C for 6 - 12 hrs. For X-Gal staining, the tissue was washed in 50 mM phosphate buffer pH 7.2 and fixed in 2.5 % glutaraldehyde by vacuum infiltration for 15 min and incubation at room temperature for 1 hr. Tissue was washed 3X in Z-buffer containing 100 mM phosphate buffer pH 7, 10 mM KCl, 1 mM $MgCl_2$ and incubated in X-Gal staining buffer (Z-buffer supplemented with 5 mM K3Fe(CN)6, 5 mM K4Fe(CN)6 and 0.08% Magenta-5-Bromo-6-chloro-3-indolyl-B-D-galactopyranoside; (X-Gal, Melford Laboratories Ltd., Ipswich, UK) or 5-Bromo-4-chloro-3-indolyl β-D-galactopyranoside (blue X-Gal, Sigma-Aldrich Company Ltd, Darmstadt Germany) at 28°C for 6-12 hrs and washed with water 3X. Subsequently, nodules and root tissue were dehydrated in an ethanol series and stored in 70% EtOH at 4°C. For imaging of whole mount tissue, stained samples were mounted on glass slides in 70% EtOH and imaged using the Keyence VHX-5000 microscope equipped with a range of zoom lenses from 20x to 1000x (Keyence Ltd, Milton Keynes, UK).

Tissue Sections

Root segments and nodules were fixed with 4% formaldehyde (Sigma-Aldrich Company Ltd, Darmstadt Germany) in 1X PBS (10X PBS contains 1.37 M NaCl, 27 mM KCl, 100 mM Na_2HPO_4, and 18 mM KH_2PO_4) with vacuum infiltration for 15 min and at 4°C overnight. The fixed material was dehydrated in an ethanol series and subsequently embedded in Technovit 7100 (Kulzer Technik, Wehrheim, Germany) according to the manufacturer's protocol. Embedded tissue was sectioned (8-10 μm) using a Leica microtome (Leica, Milton Keynes, UK), mounted on glass slides, stained in 0.1% Ruthenium Red (Sigma-Aldrich Company Ltd, Darmstadt Germany) dissolved in distilled water for 15 min and rinsed. Sections were imaged using a Zeiss Axioimager.M2 light microscope (Carl Zeiss AG, Oberkochen, Germany).

Combined 5-ethynyl-2-deoxyuridine (EdU; Invitrogen, Thermo Fisher Scientific, Waltham, USA) and modified pseudo-Schiff-propidium iodide (PI; Sigma-Aldrich Company Ltd, Darmstadt, Germany) staining, clearing and imaging was performed as previously published.[9] In addition, staining with 5-ethynyl-2-deoxyuridine (EdU; Invitrogen, Thermo Fisher Scientific, Waltham, USA) was combined with the cell wall stain Calcofluor white - Fluorescent Brightener 28 disodium salt solution (Sigma-Aldrich Company Ltd, Darmstadt, Germany). For this, roots were transferred to growth medium supplemented with 10 μM EdU and grown for 4 additional hours as previously described.[9] Subsequently, 1 cm root sections centred around the susceptibility zone were dissected and fixed in 4% formaldehyde in 1X PBS with vacuum infiltration for 15 min and incubation for 1 hr at room temperature. After 3 washes in 1X PBS, the root sections were incubated in solution containing 10 mM Alexa 488-azide (Invitrogen, Thermo Fisher Scientific, Waltham, USA) and 100 mM Tris pH 8.5 for 1 hr, followed by 30 min in solution containing 10 mM Alexa 488-azide, 100 mM Tris, 1 mM $CuSO_4$, 100 mM ascorbic acid, pH 8.5. The roots were subsequently washed in water 3X and transferred to ClearSee solution[63] for 24 – 72 hrs. For cell wall staining, root sections were transferred to ClearSee solution supplemented with 0.1% Fluorescent Brightener 28 disodium salt solution and incubated for 30 min.[63] For imaging root sections were mounted on glass slides in ClearSee solution and imaging was performed with a Zeiss 700 confocal scanning microscope using a 20X air lens objective with excitation and emission filters set to 405 nm/410–485 nm for Fluorescent Brightener 28 staining, at 488 nm/505–600 nm for EdU, and 488 nm/600-680 nm for rhizobial expressed *mCherry*, 488 nm/572–625 nm for propidium iodide (Carl Zeiss AG, Oberkochen, Germany). Images were processed using Zeiss software and FIJI.[83] GFP-tagged LSH1/LSH2 proteins expressed in hairy roots were imaged using the ClearSee protocol and confocal microscope settings as described above. Imaging data of the dual histone reporter were obtained as previously described.[32]

mRNA in situ hybridization

In situ hybridization was carried out as described previously.[91] For LSH1 and LSH2, near full length DNA fragments (400–600 bp) were amplified from GG plasmids containing the coding sequences synthesized using gene-specific forward and T7 tagged reverse primers (Table S5). The anti-sense RNA probes were synthesized by in vitro transcription using the PCR products as templates with the DIG RNA Labeling Kit (Roche). The rhizobial spot inoculated root sections were fixed in FAA (3.7% formaldehyde, 5% acetic acid, 50% ethanol) and embedded into paraffin wax in Leica ASP300 Tissue Processor. The samples were sectioned into 8μm slices. After dewaxing, rehydration and dehydration, the sections were hybridized with gene-specific probes at 55 °C overnight. After 2h washes in SSC, the slices were incubated with an anti-digoxigenin-AP antibody (Roche) for 2h at room temperature. The hybridisation signals were detected by NBT/BCIP (Roche) colour reaction. Images were taken after 24h on a Leica SP8 microscope equipped with a HC PL APO CS2 20x/0.75 NA objective and Leica DFC7000T colour camera.

Transmission electron microscopy analysis

Mature nodules of plate grown plants at 14 days post inoculation with *S. meliloti 2011* were cut from roots and immediately placed in a solution of 2.5% (v/v) glutaraldehyde in 0.05 M sodium cacodylate, pH 7.3 for fixation, and left overnight at room temperature. Samples were then placed in baskets and loaded into the Leica EM TP embedding machine (Leica, Milton Keynes, UK) using the following protocol. The fixative was washed out by three successive 15-minute washes in 0.05 M sodium cacodylate and post-fixed in 1% (w/v) OsO4 in 0.05 M sodium cacodylate for two hours at room temperature. The osmium fixation was followed by three, 15-minute washes in distilled water before beginning the ethanol dehydration series (30%, 50%, 70%, 95% and two changes of 100% ethanol, each for an hour). Once dehydrated, the samples were gradually infiltrated with LR White resin (London Resin Company, Reading, Berkshire, UK) by successive changes of resin:ethanol mixes at room temperature (1:1 for 1hr, 2:1 for 1hr, 3:1 for 1hr, 100% resin for 1 hr then 100% resin for 16 hrs and a fresh change again for a further 8 hrs) then the samples were transferred into gelatin capsules full of fresh LR White and placed at 60°C for 16 hrs to polymerize. The material was sectioned with a diamond knife using a Leica UC6 ultramicrotome (Leica, Milton Keynes, UK) and ultrathin sections of approximately 90 nm were picked up onto 200 mesh copper grids which are formvar and carbon coated (EM Resolutions, Sheffield, England). The sections were stained with 2% (w/v) uranyl acetate for 1hr and 1% (w/v) lead citrate for 1 minute, washed in distilled water and air dried. The grids were viewed in a FEI Talos 200C transmission electron microscope (FEI UK Ltd, Cambridge, UK) at 200kV and imaged using a Gatan OneView 4K x 4K digital camera (Gatan, Cambridge, UK) to record DM4 files. For overview images, sections were stained in 0.05% Toluidine Blue O for 5 min and imaged using a Leica DM6000 compound microscope 20X air objective with bright field settings (Leica Microsystems, Wetzlar, Germany).

Phylogenetic analysis

LIGHT SENSITIVE SHORT HYPOCOTYL (LSH) proteins were identified in the *Arabidopsis thaliana*, *Medicago truncatula*, *Lotus japonicus*, *Solanum lycopersicum* and *Pisum sativum* proteomes using HMMER3.1b2 HMMSEARCH (hmmer.org). The inputs to this program were the Pfam hidden Markov model (HMM), PF04852 (Pfam release 30), and the protein data sets from the genome annotations of *A. thaliana* (Araport11), *M. truncatula* (Phytozome, V10), *L. japonicus* (http://www.kazusa.or.jp/lotus/, build 3.0), *S. lycopersicum* (Phytozome, ITAG3.2) and *P. sativum* (https://urgi.versailles.inra.fr/Species/Pisum, v1a). The protein sequences detected were aligned back to the HMM using HMMER3.1b2 HMMALIGN. Gap columns in the alignment that were not part of the HMM were removed, sequences with less than 70% coverage across the alignment were removed and the longest sequence for each gene from the set of splice versions was used for phylogenetic analysis. Phylogenetic analysis was carried out using the MPI version of RAxML v8.2.9[84] with the following method parameters set: -f a, -x 12345, -p 12345, -# 100, -m PROTCATJTT. The tree was mid-point rooted and visualized using the Interactive Tree of Life (iToL) tool.[85]

QUANTIFICATION AND STATISTICAL ANALYSIS

RNA-seq

The raw FASTQ files from the RNA-sequencing experiments were first quality checked with fastQC software.[72] Then the reads were mapped to the *M. truncatula* reference genome version v5.1.9[33] using STAR (v2.7.10b).[69] The raw counts of aligned reads were calculated with featureCounts in R package Rsubread (v2.12.0).[70] To account for potential batch effects, the R sva (v3.46.0)[73] package was used and the number of surrogate variables were determined by the function sva(). Differentially expressed genes (DEGs) were identified by pairwise comparisons of raw counts of mock treatment versus experimental treatment, using the R package DESeq2 (v1.38.0)[71] while addressing the surrogate variables. The threshold for the DEGs were absolute fold change of over 1.5 and a false discovery rate (FDR) corrected p-value significance of 0.05. To account for the false positive DEGs that arise from low counts, only the genes that had DESeq2 normalized counts more or equal to 10 in at least 3 samples were analyzed. The raw RNAseq data for time-course nodulation (wildtype Jester and *nin-1*, *cre1-1* mutants) and time-course lateral root development were from previously published data,[9] deposited in National Center for Biotechnology Information Gene Expression Omnibus, with the accession number GEO: GSE13361.

Clustering and Gene Ontology enrichment analysis

The union of DEGs from the time-course nodulation RNAseq data was subjected to clustering (20,719 genes). The DEGs were clustered by their $\log_2$ fold change values across time points. The optimal number of clusters was determined by gap statistics,[92] using

the R package cluster (v2.1.4).[74] The final clusters were obtained by hierarchical k-means clustering using ward.D method and spearman correlation distance as distance measure.[93] The Gene Ontology[94] enrichment analysis was performed with topGO (v2.50.0)[75] with the significance cutoff: p-value $\leq$ 0.01. The GO term annotations and the functional annotations were obtained from *Medicago truncatula A17* r5.0 genome portal (https://medicago.toulouse.inra.fr/MtrunA17r5.0-ANR/) and this was integrated with GO terms annotated to the previous genome assembly version that was used in Schiessl et al.[9] The heatmaps were plotted with the R package ComplexHeatmap (2.14.0).[76]

ChIP-Seq

At least 3 biological replicates for each construct (*pLjUBI:GFP-LSH1*, *pLjUBI:GFP-NIN* or control *pLjUBI:NLS-GFP*) were included in the full analysis. Reads from the ChIP-sequencing experiments were provided as raw fastq data. For analysis, the ENCODE-DCC ChIP-Seq pipeline2 version 2.1.2 (https://github.com/ENCODE-DCC/chip-seq-pipeline2)[77] was used with blacklisting the chloroplast genome. Raw reads were quality-controlled and mapped to the *M. truncatula* reference genome version 5.0 (A17 r5.0, annotation version 1.9) (https://medicago.toulouse.inra.fr/MtrunA17r5.0-ANR/)[33] using Bowtie 2.[78] Duplicate reads were removed from the aligned reads with Picard MarkDuplicates (http://broadinstitute.github.io/picard). Significant peaks (q-value < 0.05) were called from aligned and deduplicated reads and annotated using macs2 and chipseeker tools, respectively. The peaks were called by macs2 with the pooled control samples and the immunoprecipitated samples as input.[79] The initial p-value threshold for peak calling was $p < 0.01$. Then they were subsequently filtered by the q-value threshold of $q < 0.05$ to correct for false discovery rate. The called peaks were annotated by ChIPseeker R package.[80] Peaks that were called in > 50% of replicates (3 out of 4 replicates in *LjUBI:GFP-LSH1*, 2 out of 3 replicates in *LjUBI:GFP-NIN*)) were merged using BEDToolsbedtools[81] and are considered as high confidence peaks. The bigwig files were generated by deepTools2 bamCompare[82] and were visualized in Medicago genome browser (https://medicago.toulouse.inra.fr/MtrunA17r5.0-ANR/).

qRTPCR

Expression values of minimum three biological replicates in three technical replicates were analyzed using the Pfaffl method with *histone H3* (*HH3*) as reference.[95] Statistical comparison was performed between WT and mutants or treatment and corresponding mock. Values depicted in bar charts are the mean of minimum 3 biological replicates ± SEM (Student's t-test; * $P < 0.05$; ** $P < 0.01$, *** $P < 0.001$).

Phenotyping

Data on the morphology of nodule primordia, rhizobial infection threads and mature nodules was depicted in bar charts and in boxplots representing the percentage of total nodule number. Total number of serrations per stipules, total number of nodules per gram root tissue and acetylene reduction rates were depicted as boxplots. Boxplots show the median (thick line), second to third quartiles (box), minimum and maximum ranges (lines), and outliers (single points). Normal distribution of data was tested using the Shapiro-Wilk normality test. For pairwise comparisons statistical analysis was performed using either unpaired Student's t-test, Wilcoxon test or Fisher's exact test. For multiple comparisons, one-way analysis of variance (one-way ANOVA) or one-way Kruskal-Wallis rank sum test, followed by Tukey multiple comparisons of means or Dunn test. The R statistical package was used for these analyses. Samples size n is provided in the figure legends and refers to the number of individual plants unless indicated otherwise. Statistical tests and significance levels are provided in the figure legends.